



# Simulations of Three 1-D Limits of the Strong-Strong Beam-Beam Interaction in Hadron Colliders Using Weighted Macro-Particle Tracking

M. Vogt\*      T. Sen†      J. A. Ellison‡

June 5, 2001

## Abstract

We develop the method of weighted macro-particle tracking (WMPT) for simulating the time evolution of the moments of the phase space densities of two beams which are coupled via the collective (strong-strong) beam-beam interaction in the absence of diffusion and damping. As an initial test we apply this method to study the  $\pi$ - and the  $\sigma$ -mode in three different 1-D limits of the beam-beam interaction. The three limits are : flat beams and transverse motion in the direction of the small width, round beams, and flat beams and motion in the direction of the large width. We have written a code (BBDemo1D) based on WMPT, which allows testing all three limits and which is suited for extension to 2 degrees of freedom.

---

\*University of New Mexico, Albuquerque, NM 87131, e-mail: [vogtm@math.unm.edu](mailto:vogtm@math.unm.edu)

†Fermilab, P.O. Box 500, Batavia, IL 60510, e-mail: [tsen@fnal.gov](mailto:tsen@fnal.gov)

‡University of New Mexico, Albuquerque, NM 87131, e-mail: [ellison@math.unm.edu](mailto:ellison@math.unm.edu)

## Contents

<b>1</b>	<b>Introduction</b>	<b>3</b>
<b>2</b>	<b>The Rotate–Kick Model</b>	<b>4</b>
2.1	The Vlasov Equation . . . . .	6
2.2	Weighted Macro–Particle Tracking . . . . .	7
2.2.1	Application of WMPT to the Rotate–Kick Model . . . . .	9
2.3	The Gaussian Source Approximation . . . . .	10
<b>3</b>	<b>1–D Models of the Beam–Beam Kick</b>	<b>11</b>
3.1	The Chao–Ruth Force . . . . .	13
3.2	The Axially Symmetric Force . . . . .	14
3.3	The Yokoya–Koiso–Zenkevich Force . . . . .	15
<b>4</b>	<b>Accuracy Considerations for WMPT</b>	<b>15</b>
<b>5</b>	<b>Simulations</b>	<b>21</b>
5.1	The dependence of the $\pi$ and $\sigma$ modes on $\Delta Q$ . . . . .	22
5.2	The dependence of the $\pi$ and $\sigma$ modes on $\Delta\xi$ . . . . .	27
<b>6</b>	<b>Conclusion and Outlook</b>	<b>27</b>
<b>7</b>	<b>Acknowledgments</b>	<b>30</b>
<b>A</b>	<b>Numerical Representation of the Yokoya–Koiso–Zenkevich Force</b>	<b>30</b>
<b>B</b>	<b>The GSA for the Yokoya–Koiso–Zenkevich Force</b>	<b>32</b>
<b>C</b>	<b>Conventions and Used Symbols</b>	<b>34</b>

# 1 Introduction

At high energy hadron colliders the need for high luminosity requires highly focused intense beams at the interaction points (IPs). These high current densities imply a strong interaction of both beams. Therefore the phase space densities of both counter rotating beams become strongly coupled. Under simplifying assumptions their evolution may be described by an integro partial differential equation, the Vlasov–equation (VE). Various methods can be used to simulate the Vlasov–evolution of the phase space densities numerically. The idea of tracking phase space densities to follow beam evolution in nonlinear fields was proposed by Kauffmann et al. [KA92]. Here we study a method which is based on computing the expectation values of functions on phase space with the time dependent density by “weighted macro–particle tracking” (WMPT). This method, to be explained in more detail in section 2.2, has the great advantage that it should be easy to implement in every reasonable multiparticle tracking code.

In the strong–strong treatment the collective force between the two beams depends on the phase space densities. Moreover, the relative strength of the beam–beam interaction depends on the particle species, the beam energies, the beam emittances, the optics at the interaction regions, the number of IPs and the phase advance between the IPs. Here we will study simplified models of the strong–strong case with one spatial degree of freedom and absorb all parameters of the beam–beam interaction into the linear beam–beam tune shift parameter  $\xi$ .

Some examples of hadron colliders (or concepts for hadron colliders) where the beam–beam interaction is considered a critical limiting factor for the luminosity are

1. LHC ( $pp$ ): Both beams are designed to have the same emittances and intensities. The spot sizes at the IPs will be the same in both planes ( $\sigma_x = \sigma_y \approx 16\mu\text{m}$ ). The beam–beam tune shift per IP will be  $\xi \approx 3.4 \cdot 10^{-3}$  [LH00].
2. Tevatron Run II ( $p\bar{p}$ ): Proton bunches are more intense than the anti–proton bunches so the anti–protons experience larger beam–beam tune shifts, about  $\xi_{\bar{p}} \approx 0.009$ . The beams are nearly round at the IP with  $\sigma \approx 33\mu\text{m}$  [TE00].
3. VLHC ( $pp$ ) / stage I : Like the LHC, the beams are designed to have identical parameters. The beams will be round and  $\xi \approx 0.002$  [VL01].
4. HERA after the luminosity upgrade: HERA is a  $e^\pm p$  collider and the electrons/positrons in principle require a Vlasov–Fokker–Planck treatment. The aspect ratio  $\sigma_x/\sigma_y$  is about 4. The linear beam–beam tune shift per IP will be for the protons  $\xi_x^{(p)} \approx 1.6 \cdot 10^{-3}$  and  $\xi_y^{(p)} \approx 0.5 \cdot 10^{-3}$  and for the leptons  $\xi_x^{(e)} \approx 0.034$  and  $\xi_y^{(e)} = 0.052$  [HO00].

Assuming bunches of length large compared to their transverse dimensions but still small compared to the  $\beta$ –functions at the IPs and no crossing angle at the IPs, the beam–beam interaction is intrinsically 2–dimensional, i.e. acts on a 4–D phase space. Nevertheless as a first step one might look at various 1–D limits which require less computing time than 2–D problems. Typically 3 different limits from 2–D to 1–D can be considered. A flat beam and motion in the “thin” direction, an axially symmetric beam and motion in a “radial” direction, and a flat beam

and motion in the “thick” direction. The first and the third limits have been studied analytically and to some extent numerically in [CR85] and [YK90, YZ93] respectively and the second limit, while turning out to be basically inconsistent, leads to a beam–beam force which is of the same form as the one used in weak–strong simulations for round beams. When studying the centroid motion of the phase space densities, two modes the sum ( $\sigma$ -mode) and the difference ( $\pi$ -mode) have been previously calculated with different characteristic frequencies, depending on the 1–D model [CR85, YK90, YZ93] or the 2–D aspect ratio [AL99, ZZ99]. One task of the initial stage of this study is to identify these two modes and see if a fully nonlinear numerical treatment yields results similar to the analytic approximations made in [CR85, YK90, YZ93]. Moreover the 2–D simulations for equal vertical and horizontal beam sizes performed in [ZZ99] can be compared to the axially symmetric limit of our 1–D simulations.

Flat beams seem more suitable for the description of  $e^\pm$  beams except perhaps for the VLHC phase II. On the other hand, the assumption of axial symmetry will, in the following, turn out to be too strong under the strong–strong premises. Therefore this first part of our study can only be seen as a starting point for further investigations. For this purpose one of the authors has developed a numerical code (BDeMo1D) that allows the simulation of all three above cases, is easily extended to 2–D and offers a wide variety of diagnostic features.

Section 2 describes the model of the ring (rotate–kick) we will be using throughout this paper and the simulation method (WMPT). Section 3 defines and describes the three 1–D limits. In section 4 the accuracy of the method is analyzed in two ways. First, the stability of an equilibrium solution of the linearized beam–beam force under the fully nonlinear evolution is discussed. Second, the effect of the re–distribution of the trajectories after many turns on the sampling of the phase space is analyzed. Section 5 contains results of our simulations with the three limits, in particular we calculate the dipole mode spectra of the beams and look for the  $\pi$ - and  $\sigma$ -modes. We examine the changes in these spectra as the tunes of the two beams are separated and also as the difference in beam–beam parameters is varied. Section 6 gives a short summary and outlook. The appendices A and B discuss technical details of the simulation for one of the three limiting 1–D cases and appendix C gives a summary of short definitions of the symbols and conventions used in this paper.

## 2 The Rotate–Kick Model

This preliminary study is restricted to interactions between 2 short, counter rotating bunches at a given IP and a linear lattice elsewhere.

The VE that governs the beam–beam interaction is formally symmetric in the two densities. Therefore we will use the notation that if  $x$  represents some quantity of “one beam”, then  $x^*$  represents the same quantity of “the other beam”.

Let  $\psi_\theta(\vec{z}) \equiv \psi_\theta(q, p)$  be the phase space density at azimuth  $\theta \in [0, \infty)$  and at the phase space point  $\vec{z} \equiv (q, p)$  and  $\rho_\theta(q) := \int_{\mathbb{R}} \psi_\theta(q, p) dp$  the density in configuration space, both normalized so that  $\int_{\mathbb{R}^2} \psi_\theta d^2z = \int_{\mathbb{R}} \rho_\theta dq = 1$  for all  $\theta$ . Let  $\theta_c$  denote the azimuth at the collision point. Then the one turn map (OTM) for turn  $m$  to  $m + 1$  at the azimuth  $\theta_c^+ + m2\pi$  directly *after* the

IP is

$$\vec{T}_m = \vec{K}[\rho_{\theta_c^- + m2\pi}^*] \circ \vec{R} \quad , \quad (2.1)$$

where  $\vec{K}[\rho_{\theta_c^- + m2\pi}^*]$  is the map for the nonlinear beam–beam kick due to the collective force which depends on the spatial density  $\rho_{\theta_c^-}^*$  of the other beam directly *before* the IP and  $\vec{R}(\vec{z}) = \underline{R}\vec{z}$ ,  $\underline{R} \in \mathbf{SP}(2)$  is the linear map from  $\theta_c^+$  to  $\theta_c^-$  of the rest of the lattice. We will often call this the *rotate–kick* model. In the following we will *suppress* the azimuth advance  $m2\pi$  from  $\theta_0 = 0$  to  $m2\pi$  in the subscripts of  $\rho$  and  $\psi$  and abbreviate  $\theta_c^- + m2\pi$  with  $\theta_c^-$  where the possible variation from turn to turn is implicitly understood. The beam–beam kick is explicitly

$$\vec{K}[\rho_{\theta_c^-}^*](q, p) = \left( \begin{array}{c} q \\ p + K[\rho_{\theta_c^-}^*](q) \end{array} \right) \quad , \quad K[\rho_{\theta_c^-}^*](q) := \zeta \int_{\mathbb{R}} G(q, q') \rho_{\theta_c^-}^*(q') dq' \quad (2.2)$$

with some model dependent kernel  $G(q, q')$  and some strength parameter  $\zeta$ . It seems reasonable to assume that  $\alpha_0 = 0$  at the IP for the unperturbed linear lattice and hence

$$\underline{R} = \left( \begin{array}{cc} \cos 2\pi Q_0 & \beta_0 \sin 2\pi Q_0 \\ -\beta_0^{-1} \sin 2\pi Q_0 & \cos 2\pi Q_0 \end{array} \right) \quad . \quad (2.3)$$

We can now precisely define our model for the evolution of the phase space density  $\psi$ . Because the OTM  $\vec{T}_m$  is symplectic, conservation of particles gives

$$\psi_{\theta_c^+ + (m+1)2\pi}(\vec{z}) = \psi_{\theta_c^+ + m2\pi}(\vec{T}_m^{-1}(\vec{z})) \quad . \quad (2.4)$$

When we discuss the accuracy of WMPT we will mean relative to the density as defined by (2.4). This can be viewed as the solution of the associated VE to be discussed in the next section. However, the VE is not well defined with a  $\delta$ –function kick as we mention in the next section.

Before proceeding we discuss the beam–beam tune shift parameter constructed by linearizing the beam–beam kick. The spatial coordinates of the two beam centroids are  $\langle q \rangle = \int_{\mathbb{R}} q \rho dq$  and  $\langle q \rangle^* = \int_{\mathbb{R}} q \rho^* dq$ . One may linearize the beam–beam kick around  $q = 0$  for head–on collisions ( $\langle q \rangle = \langle q \rangle^* = 0$ ) with symmetric densities ( $\vec{K}[\rho_{\theta_c^-}^*](0, p) = 0$ ) yielding  $\vec{K}[\rho_{\theta_c^-}^*](\vec{z}) = \underline{K}\vec{z} + O(\vec{z}^2)$  where

$$\underline{K} := \left( \begin{array}{cc} 1 & 0 \\ \kappa[\rho_{\theta_c^-}^*] & 1 \end{array} \right) \quad , \quad \kappa[\rho_{\theta_c^-}^*] := \left. \frac{d}{dq} K[\rho_{\theta_c^-}^*] \right|_{q=0} \quad . \quad (2.5)$$

The Jacobian of the OTM in (2.1) is then  $\underline{T} = \underline{K}\underline{R}$  and a stable solution of the linearized motion exists iff  $|\cos 2\pi Q_0 + \frac{\kappa\beta_0}{2} \sin 2\pi Q_0| < 1$ . Then, using the Courant–Snyder functions of the linearly perturbed lattice  $\alpha, \beta, \gamma$  and the linearly perturbed tune  $Q$ , the Jacobian of the OTM can be brought to the standard form

$$\underline{T} = \left( \begin{array}{cc} \cos 2\pi Q + \alpha \sin 2\pi Q & \beta \sin 2\pi Q \\ -\gamma \sin 2\pi Q & \cos 2\pi Q - \alpha \sin 2\pi Q \end{array} \right) \quad (2.6)$$

where

$$Q = \frac{1}{2\pi} \arccos \left( \cos 2\pi Q_0 + \frac{\kappa\beta_0}{2} \sin 2\pi Q_0 \right) \quad (2.7a)$$

$$= Q_0 - \frac{\kappa\beta_0}{4\pi} + O(\kappa^2\beta_0^2) \quad (2.7b)$$

$$\beta = \beta_0 \frac{\sin 2\pi Q_0}{\sin 2\pi Q} , \quad \alpha = -\frac{\kappa}{2}\beta , \quad \gamma = \frac{1}{\beta} + \frac{\kappa^2\beta}{4} . \quad (2.7c)$$

This analysis contains the parameter  $\kappa$  which depends on  $\rho_{\theta_c^*+m2\pi}^*$  which in principle must be assumed to be changing from turn  $m$  to turn  $m+1$  because of the nonlinear collective beam-beam interaction. Nevertheless it gives an intuitive interpretation of the *initial* strength of a beam-beam interaction in the sense that the *beam-beam tune shift parameter*  $\xi$  is defined by

$$Q \Big|_{m=0} - Q_0 = \xi + O(\kappa^2\beta^2) , \quad \xi := -\frac{\kappa[\rho_{\theta_c^*}^*]\beta_0}{4\pi} . \quad (2.8)$$

Note that a positive (defocusing)  $\kappa$ , like it is in the case of *pp*-interactions, results in a negative tune shift parameter.

## 2.1 The Vlasov Equation

In the absence of damping and diffusion the phase space densities  $\psi_\theta$  and  $\psi_\theta^*$  evolve according to the coupled Vlasov equations<sup>1</sup> (VE)

$$\partial_\theta \psi + \partial_q \psi \cdot \partial_p H - \partial_p \psi \cdot \partial_q H = 0 \quad (2.9a)$$

$$\partial_\theta \psi^* + \partial_{q^*} \psi^* \cdot \partial_{p^*} H - \partial_{p^*} \psi^* \cdot \partial_{q^*} H = 0 \quad (2.9b)$$

where

$$H[\psi, \psi^*](\vec{z}, \vec{z}^*, \theta) = H_0(\vec{z}, \theta) + H_0^*(\vec{z}, \theta) + \delta_{2\pi}(\theta - \theta_c) \left( H_1[\psi_{\theta_c^*}^*](\vec{z}) + H_1^*[\psi_{\theta_c}](\vec{z}^*) \right) \quad (2.10)$$

is the Hamiltonian including the collective force and  $\delta_{2\pi}$  is the  $2\pi$ -periodic  $\delta$ -function assuming one IP. Note that that  $H_1$  depends on the densities directly before the collision. This Hamiltonian is equivalent to the rotate-kick model (2.4) we are going to use. If  $H_1$  contained  $\psi_\theta$  (or  $\psi_\theta^*$ ), the resulting VE would not be well defined since the  $\delta$ -function would be multiplied with  $\partial_q H_1$  which is discontinuous at  $\theta \bmod 2\pi = \theta_c$ . However, in a real accelerator the beam-beam interaction takes place over a small finite range in azimuth and the  $\delta$ -function is replaced with a regular distribution in  $\theta$ . A finite interaction length would then lead to a thick-lens representation of the beam-beam interaction. Moreover note that the asterisks on  $H_0$  and  $H_1$  reflect the fact that in our model “the other beam” may have a different unperturbed tune  $Q_0^*$  and beam-beam tune shift parameter  $\xi^*$ .

In order to obtain complete knowledge of the coupled multiparticle system one needs, in principle, to solve the VE. Numerous analytical approximations and numerical simulation methods exist and have been applied to the strong-strong beam-beam interaction. To mention only some of the numerical approaches:

---

<sup>1</sup>This is the last time we write equations for the “unstarred” and “starred” beam.

1. Standard PDE solvers (divided difference schemes).
2. Particle-in-cell (PIC) codes [AN98, KR00].
3. The Perron-Frobenius (PF) operator method [WE00, EW01].
4. Weighted macro-particle tracking (yields moments of the distribution).

The first two methods are well known and will not be discussed here.

The PF operator method employs the conservation of the phase space density along trajectories according to (2.4). Given a map  $\vec{T}$ , the action of the PF operator  $\mathfrak{T}$  on a density  $\psi$  is simply

$$\mathfrak{T} \psi(\vec{z}) = \psi(\vec{T}^{-1}(\vec{z})) \quad (2.11)$$

and thus (2.4) yields

$$\psi_{\theta_c^+ + (m+1)2\pi} = \mathfrak{T} \psi_{\theta_c^+ + m2\pi} \quad . \quad (2.12)$$

The action of  $\mathfrak{T}$  is completely defined by the map  $\vec{T}$ . Now the densities and  $\mathfrak{T}$  are discretized on a square  $n \times n$  grid in phase space, the density being defined at off-grid points by local polynomial interpolation. The kick is calculated at grid points from values of the density at grid points. Note that the kick  $\vec{K}$  depends only on  $q$  and that the kernel  $K$  acts on the spatial density  $\rho(q)$  so that the computation of the kick for all  $N := n^2$  grid points is obtained by the multiplication of an  $n$ -vector with an  $n \times n$ -matrix and thus is an  $O(N)$  operation ! Then  $\psi_{\theta_c^+ + m2\pi}(\vec{T}_m^{-1}(\vec{z}))$  is computed for grid points  $\vec{z}$  by interpolation to give an update of  $\psi$  on grid points. Note that the interpolation implies an intrinsic smoothing of the representation of the density on the grid at every step. The PF method has been shown to be stable for the Vlasov-Fokker-Planck equation (using operator splitting to handle the Fokker-Planck part) in beam physics [WE00, EW01]. Moreover its main premise, the conservation of the density along trajectories, is also a key concept for the method of WMPT.

## 2.2 Weighted Macro-Particle Tracking

Let  $f(\vec{z})$  be a (integrable) function on phase space. Then its average at azimuth  $\theta$  is defined as

$$\begin{aligned} \langle f \rangle_\theta &:= \int_{\mathbb{R}^2} f(\vec{z}) \psi_\theta(\vec{z}) d^2 z \\ &= \int_{\mathbb{R}^2} f(\vec{z}) \psi_0(\vec{M}_\theta^{-1}(\vec{z})) d^2 z \\ &= \int_{\mathbb{R}^2} f(\vec{M}_\theta(\vec{z})) \psi_0(\vec{z}) d^2 z \end{aligned} \quad (2.13a)$$

where  $\vec{M}_\theta$  is the map from 0 to  $\theta$  and where in the third equality we have used the fact that the determinant of the Jacobian of a symplectic map is one. In this study  $f$  is chosen to be either the (sufficiently regular) kernel of the collective force  $f_q(\vec{z}') := G(q, \mathfrak{X} \vec{z}')$ , where the projector  $\mathfrak{X}$  is defined via  $\mathfrak{X} \vec{z} := q$ , or a  $(v+w)$ -th order monomial  $f_{v,w}(\vec{z}) := q^v p^w$  of the beam distribution.

In the first case the average  $\langle f_q \rangle_{\theta \bar{c}}$  is the beam beam kick exerted by the “unstarred” beam on the “starred” beam and in the second case  $\langle f_{v,w} \rangle_{\theta}$  is a  $(v+w)$ -th order moment of the phase space distribution of the “unstarred” beam. The averages  $\langle f_q \rangle_{\theta \bar{c}}^*$  and  $\langle f_{v,w} \rangle_{\theta}^*$  are analogously defined. Eq. (2.13a) means that in order to compute the expectation value of  $f$  it suffices to compute  $\langle f \circ \vec{M}_{\theta} \rangle_0$  or algorithmically speaking that:

For some representation of  $\psi_0$  on a (not necessarily square) initial mesh  $\{\vec{z}_{ij}\}_{\substack{1 \leq i \leq n_q \\ 1 \leq j \leq n_p}}$ , an approximation of  $\langle f \rangle_{\theta}$  is given

$$\langle f \rangle_{\theta} \approx \sum_{i,j=1}^{n_q, n_p} w_{ij} \psi_0(\vec{z}_{ij}) f(\vec{M}_{\theta}(\vec{z}_{ij})) \quad , \quad (2.14)$$

where the  $w_{ij}$  are the weights of the quadrature formula.

In this study an initially square mesh with  $n_q = n_p =: n$ ,  $q_{i-1} - q_i = \Delta_q$ ,  $p_{j-1} - p_j = \Delta_p$  for all  $i, j$  and the Gaussian mid-point rule have been used so that the *quadrature* weights are particularly simple:  $w_{ij} =: w = \Delta_q \Delta_p$ . Note that once the *total* weights

$$\mathfrak{W}_{ij} := w_{ij} \psi_0(\vec{z}_{ij}) \quad (2.15)$$

are assigned to every trajectory

$$\vec{\eta}_{ij}(\theta) := \vec{M}_{\theta}(\vec{z}_{ij}) \quad (2.16)$$

starting at  $\vec{z}_{ij}$ , the double index  $ij$  can be replaced by one linear index  $k$  since the result of a finite sum does not depend on the ordering of the terms. This *weighted macro-particle tracking* (WMPT) procedure only requires forward tracking of macro-particles and as a byproduct to the distribution moments it produces  $N := n^2$  particle trajectories and the associated Poincaré sections, etc. Moreover the conservation of probability is guaranteed by construction (set  $f \equiv 1$  in (2.14)).

It has been shown for an example of the VE taken from plasma-physics [WO96, WO99, WO00], that for fixed  $\theta$  the trajectories obtained by WMPT converge at least linearly in  $\Delta_q + \Delta_p + \Delta_{\theta}$  to the exact trajectories of the Hamiltonian system (2.10). However, the upper bounds on the error given in [WO96, WO99, WO00] depend exponentially on  $\theta$  and are thus not of great use in the case of multiturn tracking.

Finally it should be mentioned that with WMPT one *can* obtain an approximation of the phase space density. Let  $\{\vec{z}_{\mu\nu} := (q_{\mu}, p_{\nu})\}_{\substack{1 \leq \mu \leq \tilde{n}_q \ll n \\ 1 \leq \nu \leq \tilde{n}_p \ll n}}$  be a uniform rectangular mesh and

$$\chi_{\mu\nu}(\vec{z}) := \begin{cases} 1 : q_{\mu} - \frac{\Delta_q}{2} < q \leq q_{\mu} + \frac{\Delta_q}{2} \ \& \ p_{\nu} - \frac{\Delta_p}{2} < p \leq p_{\nu} + \frac{\Delta_p}{2} \\ 0 : \text{otherwise} \end{cases} \quad (2.17)$$

be the indicator function of the rectangular “bins”  $\mathcal{R}_{\mu\nu} := (q_{\mu} - \frac{\Delta_q}{2}, q_{\mu} + \frac{\Delta_q}{2}] \times (p_{\nu} - \frac{\Delta_p}{2}, p_{\nu} + \frac{\Delta_p}{2}]$ . These indicator functions define a partitioning of unity, in the sense that  $\sum_{\mu,\nu} \chi_{\mu\nu}(\vec{z}) = 1$  for all  $\vec{z}$ . Then

$$\langle \chi_{\mu\nu}(\vec{z}) \rangle_{\theta} = \int_{\mathcal{R}_{\mu\nu}} \psi_{\theta}(\vec{z}) d^2 z = \int_{\mathbb{R}^2} \chi_{\mu\nu}(\vec{z}) \psi_{\theta}(\vec{z}) d^2 z \approx \sum_{i,j} \mathfrak{W}_{ij} \chi_{\mu\nu}(\vec{\eta}_{ij}(\theta)) \quad (2.18)$$

is an approximation of  $\psi_\theta$  on the mesh defined by  $\{\bar{z}_{\mu\nu}\}$ . The effective smoothness of this approximation depends on the average number of macro-particles in each “bin”. Therefore the mesh defined by the  $\bar{z}_{\mu\nu}$  has to be coarser than the initial mesh defined by the  $\bar{z}_{ij}$ . In section 4 we will make use of this *mesh projection* to qualitatively discuss the stability of WMPT. Note that instead of the indicator function  $\chi_{\mu\nu}$  we could have used any other partitioning of unity which reflects the mesh structure.

### 2.2.1 Application of WMPT to the Rotate-Kick Model

Let  $\bar{\eta}_{ij}(\theta_c^+ + 2\pi(m-1))$  and  $\bar{\eta}_{ij}^*(\theta_c^+ + 2\pi(m-1))$  be given. Then  $\bar{\eta}_{ij}(\theta_c^- + 2\pi m) = \underline{R}\bar{\eta}_{ij}(\theta_c^+ + 2\pi(m-1))$  and  $\bar{\eta}_{ij}^*(\theta_c^- + 2\pi m) = \underline{R}^*\bar{\eta}_{ij}^*(\theta_c^+ + 2\pi(m-1))$  give the phase space position of the  $(ij)$ -th particle of each beam just before the kick. The kick on a particle of the “unstarred” beam at position  $q_{ij} := \mathfrak{X}\bar{\eta}_{ij}(\theta_c^- + 2\pi m)$  is given by

$$\begin{aligned} K[\rho_{\theta_c^- + 2\pi m}^*](q_{ij}) &= \zeta \int_{\mathbb{R}^2} G(q_{ij}, \mathfrak{X}\bar{z}') \psi_{\theta_c^- + 2\pi m}^*(\bar{z}') d^2 z' \\ &= \zeta \int_{\mathbb{R}^2} G(q_{ij}, \mathfrak{X}\bar{z}') \psi_0^* \left( \vec{M}_{\theta_c^- + 2\pi m}^{*-1}(\bar{z}') \right) d^2 z' \\ &= \zeta \int_{\mathbb{R}^2} G \left( q_{ij}, \mathfrak{X}\vec{M}_{\theta_c^- + 2\pi m}^*(\bar{z}') \right) \psi_0^*(\bar{z}') d^2 z' . \end{aligned} \quad (2.19)$$

We then approximate the kick by

$$K[\rho_{\theta_c^- + 2\pi m}^*](q_{ij}) \approx K\{\bar{\eta}^*\}_{\theta_c^- + 2\pi m}(q_{ij}) := \zeta \sum_{k,l=1}^n G(q_{ij}, \mathfrak{X}\bar{\eta}_{kl}^*(\theta_c^- + 2\pi m)) \mathfrak{W}_{kl}^* . \quad (2.20)$$

The phase space positions after the kick are thus

$$\begin{aligned} \bar{\eta}_{ij}(\theta_c^+ + 2\pi m) &= \vec{K}\{\bar{\eta}^*\}_{\theta_c^- + 2\pi m}(\bar{\eta}_{ij}(\theta_c^- + 2\pi m)) \\ \bar{\eta}_{ij}^*(\theta_c^+ + 2\pi m) &= \vec{K}\{\bar{\eta}\}_{\theta_c^- + 2\pi m}(\bar{\eta}_{ij}^*(\theta_c^- + 2\pi m)) \end{aligned} \quad (2.21)$$

where  $\vec{K}\{\bar{\eta}^*\}_\theta$  is the kick map (2.2) with  $K[\rho_{\theta_c^- + 2\pi m}^*]$  replaced by  $K\{\bar{\eta}^*\}_{\theta_c^- + 2\pi m}$  according to (2.20).

Note that the kicks must be calculated at  $N := n^2$  positions  $q_{ij}$  and that the calculation of  $K\{\bar{\eta}^*\}(q)$  for fixed  $q$  takes in principle  $N$  evaluations of the kernel  $G(q_{ij}, \mathfrak{X}\bar{\eta}_{kl}^*)$  and  $N$  multiplications with the total weights  $\mathfrak{W}_{kl}$ . Therefore the kicks require in principle  $O(N^2)$  flops where  $N$  is the number of macro-particles tracked. Moreover, in particular for 2-D motion ( $N \rightarrow n^4$ ), which is the long term goal of this study anyway, special care has to be taken to avoid  $O(N^2) = O(n^8)$  methods. Nevertheless, this is the worst case since for *certain* models of beam-beam interactions, in 1-D (see section 3.1) as well as in 2-D [GE88], there are more efficient methods to compute the collective force than the  $O(N^2)$  methods.

Let  $\Delta_q = \Delta_p =: \Delta$ . Then the quadrature error is bounded by  $C\Delta^s \|\vec{M}_\theta\|$  where  $s$  depends on the smoothness of the integrand and the order of the quadrature formula,  $\|\vec{M}_\theta\|$  is some

derivative norm of  $\vec{M}_\theta$  and  $C$  is a constant independent of  $\Delta$  and  $\vec{M}_\theta$ . It is to be expected that  $\|\vec{M}_\theta\|$  increases with  $\theta$  and so it is natural to ask what is the optimal  $\Delta$  for a given interval  $\theta \in [0, \Theta]$ . Our trajectory calculations indicate that in a typical setup as in section 5, particles which are started inside  $1 \sigma_0$  fill that region densely. Thus two particles which start  $2 \sigma_0$  apart can become close and this can give a jaggedness to an initially smooth density (since trajectories carry their initial density with them, see (2.4), (2.15) and (2.16)).

However, the situation is not as bad as it might seem since we are calculating expectation values which potentially can average out any fast oscillating part present in  $\vec{M}_\theta$ . We are investigating optimal  $\Delta$  for fixed  $\Theta$  and will report that elsewhere.

Finally we compute phase space averages via

$$\langle f \rangle_\theta \approx \sum_{i,j} \mathfrak{W}_{ij} f(\vec{\eta}_{ij}(\theta)) \quad , \quad \langle f \rangle_\theta^* \approx \sum_{i,j} \mathfrak{W}_{ij}^* f(\vec{\eta}_{ij}^*(\theta)) \quad . \quad (2.22)$$

This is an  $O(N)$  calculation and thus is not an important factor in the flop count, as long as the flop count of the kick computation is of higher order in  $N$ . The quadrature error in the calculation of the averages can be discussed as above, however the pessimistic view is ameliorated by the inherent smoothing due to integration.

If the integrand can be guaranteed to be sufficiently moderately varying, then WMPT, in contrast to methods that require an explicit mesh at each time step, has the advantage that the mesh layout depends *only* on the *initial* conditions. As an example consider a strictly linear OTM, in particular no beam-beam interaction and an initial beam distribution with an offset w.r.t. the origin (closed orbit) of say  $x\sigma_0$  in normalized coordinates. Then in an explicit mesh method one requires a mesh that is large enough to contain not only the initial distribution up to some reasonable cut-off (say  $c\sigma_0$ ) but to contain a circle of  $(x+c)\sigma_0$ . Alternatively, if one wants to keep a smaller mesh, one has to recompute the mesh every time step or every few time steps. For the linear case WMPT has been tested with a large initial offset and an initial mesh centered around the beam centroid with width  $c\sigma_0$ . In this case WMPT carries its mesh along with the trajectories and the moments computed with WMPT were close to those computed analytically using (2.4) to a very high precision.

### 2.3 The Gaussian Source Approximation

In the previous section we have seen that WMPT might become time consuming due to the loss of the mesh structure and inaccurate due to the build up of rapid variations in  $\psi_0(\vec{z})f(\vec{M}_\theta(\vec{z}), \theta)$ . These rapid variations would be averaged away in an exact integration but might degrade the accuracy of the result of the numerical quadrature. In particular errors in the computation of the collective beam-beam kick can become dangerous since they can corrupt the complete dynamics of the coupled two beam system. There is a method [FU98] which smoothes the distribution as far as the collective force is concerned and at the same time makes its computation  $O(N)$ . The method simply consists of computing some set of moments  $\{\langle q^k \rangle_\theta^*\}$  of the actual distribution and inserting them as parameters in an *analytic* formula for the beam-beam kick assuming some

test density  $\tilde{\rho}$

$$\tilde{K}(q; \{\langle q^k \rangle_{\theta_c^-}^*\}) := \int_{\mathbb{R}} G(q, q') \tilde{\rho}(q'; \{\langle q^k \rangle_{\theta_c^-}^*\}) dq' \quad . \quad (2.23)$$

The form of the “starred” test density in the computation of the collective form stays fixed — only the change of the parameters reflects the evolution of the density of the other beam. This method is not completely consistent with Vlasov evolution since in general the form of  $\rho_{\theta_c^-}^*(q^*)$  is different from  $\tilde{\rho}(q^*; \{\langle q^k \rangle_{\theta_c^-}^*\})$ . Nevertheless it has the benefit of intrinsic smoothing (with suitably chosen  $\tilde{\rho}$ ) and allows the simulation of the evolution with a much larger number of macro-particles at a still reasonable computation time. Even then it is still not clear which shape  $\tilde{\rho}$  should have and in principle the results to be presented in section 5 suggest that it is not a Gaussian shape. However, as starting point for this study, whenever we have approximated the collective kick by Eq. (2.23), we have chosen  $\tilde{\rho}$  to be a Gaussian

$$\tilde{\rho}(q; \mu, \sigma) = \frac{1}{\sqrt{2\pi} \sigma} e^{-\frac{(q-\mu)^2}{2\sigma^2}} \quad . \quad (2.24)$$

In the following we will call (2.23) with  $\tilde{\rho}$  defined by (2.24) the *Gaussian source approximation* (GSA). This approximation is also called the “quasi-strong-strong” or “soft Gaussian” approximation. We want to stress the point that in the GSA the evolution of the densities of the two beams are *not* faked by some phenomenological evolution law for the parameters  $\mu$  and  $\nu$  of a Gaussian but that they evolve according to (2.4) with a modified collective kick. Only the collective beam-beam kick is approximated. This method (together with tracking an initially Gaussian ensemble of macro-particles of *identical* weight) has been used in 2-D to compute the frequencies of the  $\pi$ - and  $\sigma$ -modes with various aspect ratios  $\sigma_x/\sigma_y$  [ZZ99].

In sections 4 and 5 we will use ensembles of macro-particles, initially on a uniform orthogonal mesh and with Gaussian weights  $\mathfrak{W}_{ij}$ , to study the evolution of the distribution moments employing WMPT with and without the additional Gaussian source approximation.

### 3 1-D Models of the Beam-Beam Kick

As pointed out in the introduction, one may take at least 3 different limits when breaking down the 2-D beam-beam interaction into 1-D models.

1. The Chao-Ruth (CR) limit [CR85]: The beams at the IP are assumed to be flat, e.g.  $\sigma_x \gg \sigma_y$  and the motion is studied in the phase plane associated with  $y$  :

$$K_{\text{cr}}[\rho_{\theta_c^-}^*](y) = \zeta \int_{\mathbb{R}} \text{sgn}(y - y') \rho_{\theta_c^-}^*(y') dy' \quad . \quad (3.25)$$

2. The axially symmetric (AS) limit: The beams are assumed to be round, i.e.  $\sigma_x = \sigma_y$ , and the motion w.r.t. an arbitrary transverse direction ( $r$ ) is studied :

$$K_{\text{as}}[\rho_{\theta_c^-}^*](r) = \frac{\zeta}{r} \int_0^r \rho_{\theta_c^-}^*(r') r' dr' \quad . \quad (3.26)$$

3. The Yokoya–Koiso–Zenkevich (YO) limit [YK90, YZ93]: Again the beams are assumed to be flat, e.g.  $\sigma_x \gg \sigma_y$  but the motion *in* the phase plane associated with  $x$  is studied :

$$K_{\text{yo}}[\rho_{\theta_c}^*](x) = \zeta \mathcal{P} \int \frac{\rho_{\theta_c}^*(x')}{(x - x')} dx' \quad (3.27)$$

where  $\mathcal{P}$  denotes the Cauchy principal value.

Fig. 1 shows the three limits of beam–beam kick  $K[\rho](q)$  for a standard Gaussian density  $\rho(q; 0, 1)$  and for  $\zeta$  chosen so that the slope at the origin is unity (i.e.  $\kappa[\rho] = 1$ ).

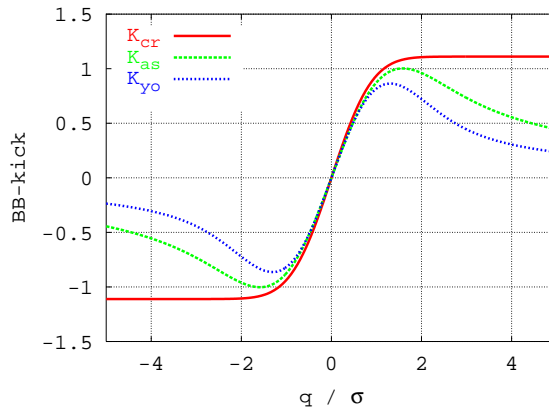


Figure 1: (color) The beam–beam kicks  $K_{\text{cr}}[\rho](q)$ ,  $K_{\text{as}}[\rho](q)$  and  $K_{\text{yo}}[\rho](q)$  for a standard Gaussian  $\rho(q; 0, 1)$ . In all three cases  $\kappa[\rho]$  is chosen to be 1.

We note that the Chao–Ruth as well as the Yokoya–Koiso–Zenkevich limit seem to be more suited for  $e^\pm$ -colliders. In the  $ep$ -collider HERA the ratio  $\sigma_y/\sigma_x$  of  $e^\pm$ -beam is increased at the IP to about 1/4 by allowing a larger vertical than horizontal  $\beta$ -function.

On the other hand, as it will turn out later, the assumption of axial symmetry is too strong and therefore possibly not a realistic model of two hadron beams coupled by the collective beam–beam force.

In the following three subsections we will discuss the three limits in more detail and in particular derive the explicit dependence of the tune shift parameter  $\xi$  on the strength parameter  $\zeta$  (see (2.2)) under the assumption of an *initially* Gaussian beam. Then  $\xi(\zeta)$  can be inverted to obtain the strength for the beam–beam tune shift parameter in the “physical parameters” of a practical collision scheme

$$\xi_{x,y} = \frac{r_p N^* \beta_{x,y}}{2\pi \gamma_L \sigma_{x,y} (\sigma_x + \sigma_y)} \quad (3.28)$$

where  $r_p$  is classical particle radius,  $\gamma_L$  is the Lorentz factor and  $N^*$  is the number of particles in the other bunch. Moreover we will derive the form of the beam–beam kick in the GSA  $\tilde{K}(q; \mu_{\theta_c}^*, \sigma_{\theta_c}^*)$ . The techniques to obtain  $\xi(\zeta)$  and  $\tilde{K}$  are formally identical. The only difference

is that the initial density  $\rho_{\theta_c^-}^*(q)$  that is used to compute  $\xi(\zeta)$  is replaced by the test density  $\tilde{\rho}(q^*; \mu_{\theta_c^-}^*, \sigma_{\theta_c^-}^*)$  to obtain the GSA. In the following we will denote both densities by  $\rho(q; \mu^*, \sigma^*)$ .

### 3.1 The Chao–Ruth Force

In the Chao–Ruth case the kick is given by (3.25). The Chao–Ruth model can be considered as a 1–D Poisson problem  $K_{\text{cr}}[\rho](q) = \zeta \int_{\mathbb{R}} \partial_q \tilde{G}(q, q') \rho(q') dq'$ . Here  $\tilde{G}(q, q') := |q - q'|$  is the 1–D Green’s function which fulfills  $\partial_q^2 \tilde{G}(q, q') = 2\delta(q - q')$ . Therefore the integral kernel  $G(q, q')$  for the CR beam–beam kick can be identified with  $\partial_q \tilde{G}(q, q') = \text{sgn}(q - q')$ .

It follows immediately from the form of the kernel that the CR kick on a particle at  $q$  is proportional to the number of particles of beam  $*$  at a spatial position less than  $q$  minus the number of particles at a spatial position larger than  $q$ . In particular we find  $\lim_{q \rightarrow \pm\infty} K_{\text{cr}}[\rho](q) = \mp\zeta \neq 0$ . This appears unphysical only at first sight. Since we assume flat beams and motion in the perpendicular plane, the charge distribution of the macro–particles of beam  $*$  are actually represented by planes of constant planar density. Similar to the case of a capacitor with infinitely large plates the field on a test particle due to each of the charge planes does not depend on the distance of the particle to the plane.

Moreover the simple structure of the CR kernel  $G$  allows the computation of the beam–beam kick on  $N$  macro–particles exerted by an ensemble of  $N^* \approx N$  particles, both located at arbitrary position in configuration space, with *less* than  $O(N^2)$  operations. We can order the  $N + N^*$  particles in sequence of increasing  $q$ . This can be done, for example by the HEAPSORT algorithm [NR92], at an expense of  $O(N \log N)$ . Then one starts with the “leftmost” particle which receives a kick of  $-\zeta$ , the next particle receives a kick of  $-\zeta$  if it belongs to the same beam as the “leftmost” particle or  $-\zeta(1 - \mathfrak{W}_l)$  if it belongs to the other beam, and so on. Here  $\mathfrak{W}_l$  is the weight of the “leftmost” particle. This last step only has an operations count of  $O(N)$  so that the total asymptotic order count of the algorithm is determined by the sorting and hence  $O(N \log N)$ .

With the Gaussian density  $\rho(q; \mu^*, \sigma^*) := 1/(\sqrt{2\pi}\sigma^*) \exp\left(-\frac{(q-\mu^*)^2}{2\sigma^{*2}}\right)$  we find

$$\begin{aligned} K_{\text{cr}}[\rho](q) &= \zeta \int \text{sgn}(q - q') \rho(q'; \mu^*, \sigma^*) dq' \\ &= \zeta \left( 2 \text{erf}\left(\frac{q - \mu^*}{\sigma^*}\right) - 1 \right) \end{aligned} \quad (3.29)$$

where we define  $\text{erf}(q) := \int_{-\infty}^q \rho(q'; 0, 1) dq'$ . This formula describes the nonlinear beam–beam kick in the GSA and determines  $\xi(\zeta)$  for initially Gaussian beams. From Eq. (2.5) and  $\frac{d}{dq} K_{\text{cr}}[\rho] = 2\zeta \rho(q; \mu^*, \sigma^*)$  we find

$$\xi_{\text{cr}} := \frac{\beta_0 \frac{d}{dq} K_{\text{cr}}[\rho] \Big|_{q=\mu^*=0}}{4\pi} = (2\pi)^{-3/2} \frac{\zeta \beta_0}{\sigma^*} . \quad (3.30)$$

### 3.2 The Axially Symmetric Force

In the axially symmetric case the kick is given by (3.26). Assume infinitely long axially symmetric bunches in both beams, i.e. in cylindrical coordinates with origin at  $\langle(x, y)\rangle$  the spatial density fulfills  $\partial_z \rho = \partial_\phi \rho = 0$ . Note that the centroid of the beams are not demanded to be on the closed orbit nor are they demanded to be at identical for both beams. The beam-beam force after a Lorentz boost into the rest frame of the source beam is then given by the electric field  $\vec{E} =: E(r)\hat{r}$  where  $\hat{r}$  is the radial unit vector and  $r = \sqrt{x^2 + y^2}$ . Gauss' law yields for any cylinder  $\mathcal{Z}$  with radius  $r$  and length  $\Delta_l$

$$\begin{aligned} \int_{\partial\mathcal{Z}} \vec{E} \cdot \hat{n} dS &= \Delta_l 2\pi r E \\ &= \int_{\mathcal{Z}} \rho(r) dV = \Delta_l 2\pi \int_0^r \rho(r') r' dr' \end{aligned} \quad (3.31)$$

where  $\hat{n}$  is the unit vector normal to  $\partial\mathcal{Z}$  and thus  $E(r) = 1/r \int_0^r \rho(r') r' dr'$ . Undoing the Lorentz boost and absorbing all constants into  $\zeta$  we find (3.26). We can then, under the premise that the beam stays round, choose an arbitrary transverse direction for  $\hat{r}$ . This procedure is applied usually to the strong source beam in weak-strong simulations.

Unfortunately under the full Vlasov evolution the assumption of axial symmetry is not selfconsistent. For a 1-D model this means that the consistency constraint that the density is left-right symmetric about the centroid ( $\rho_\theta(\langle q \rangle_\theta + q') = \rho_\theta(\langle q \rangle_\theta - q') \quad \forall q'$ ) is in general not fulfilled for all  $\theta$ . In particular the above constraint implies that all *odd* order centered moments  $\langle (q - \langle q \rangle)^{2n+1} \rangle_\theta$  vanish identically. In order to obtain a selfconsistent 1-D approximation of a round beam we modify the beam-beam kick to use the *symmetrized* density  $\frac{1}{2}(\rho_\theta(\langle q \rangle_\theta + q') + \rho_\theta(\langle q \rangle_\theta - q'))$ . This is equivalent to taking the averaging of  $\rho_\theta(\langle q \rangle_\theta + x)$  at  $+q'$  and at  $-q'$ . Thus we can write the beam-beam kick

$$K_{\text{as}}[\rho_{\theta_c}^*](q) = \frac{1}{q - \langle q \rangle_{\theta_c}^*} \int_{-|q - \langle q \rangle_{\theta_c}^*|}^{+|q - \langle q \rangle_{\theta_c}^*|} \rho^*(\langle q \rangle_{\theta_c}^* + q') |q'| dq' \quad . \quad (3.32)$$

One can easily see that for any  $\rho$  such that  $\langle |q| \rangle$  exists, the limit  $q \rightarrow \pm\infty$  of  $K_{\text{as}}[\rho](q)$  vanishes at least linearly with  $1/|q - \langle q \rangle^*|$ .

The kernel for the AS beam-beam kick is

$$\begin{aligned} G(q, q') &= \frac{1}{q - \langle q \rangle_{\theta_c}^*} \chi(\langle q \rangle_{\theta_c}^*, q, q') |q' - \langle q \rangle_{\theta_c}^*| \\ \chi(\mu, q, q') &:= \begin{cases} 1 & : |q' - \mu| < |q - \mu| \\ 0 & : |q' - \mu| \geq |q - \mu| \end{cases} \quad . \end{aligned} \quad (3.33)$$

Note that here the kernel itself depends on the first moment of  $\rho_{\theta_c}^*$ .

With a Gaussian density  $\rho(q'; \mu^*, \sigma^*)$  as in section 3.1 the beam-beam kick is

$$K_{\text{as}}[\rho](q) = \sqrt{\frac{2}{\pi}} \zeta \frac{\sigma^*}{q - \mu^*} \left( 1 - e^{\left( -\frac{(q - \mu^*)^2}{2\sigma^{*2}} \right)} \right) \quad . \quad (3.34)$$

And analogously to section 3.1

$$\xi_{\text{as}} = \frac{\zeta}{2} (2\pi)^{-3/2} \frac{\beta_0}{\sigma^*} . \quad (3.35)$$

As yet, no algorithm for computing the exact AS beam–beam kick (3.32) at a lower order count than  $O(N^2)$  has been found. However, the preliminary numerical results of this study, to be presented in section 5, seem to indicate that once the axial symmetry is put in by hand, the additional assumption of a Gaussian source does not change the moment calculation significantly.

### 3.3 The Yokoya–Koiso–Zenkevich Force

In the Yokoya–Koiso–Zenkevich case the kick is given by (3.27). The Yokoya–Koiso–Zenkevich force has been derived [YK90] from the limit  $\sigma_x \gg \sigma_y$  in the integral that solves the 2–D Poisson–problem

$$K_{\text{yo}}[\rho](x) = \zeta \lim_{\sigma_y/\sigma_x \rightarrow 0} \int_{\mathbb{R}^2} \partial_x \tilde{G}(x, y, x', y') \rho^{(2)}(x', y') dx' dy' \quad (3.36)$$

where  $\tilde{G}(x, y, x', y')$  is the 2–D Green’s function  $\log(\sqrt{(x-x')^2 + (y-y')^2})$ . Its kernel is singular and therefore a more careful treatment of the Yokoya–Koiso–Zenkevich force in the context of WMPT is needed. We do this in appendix A and note here only that the Cauchy principle value is not very well represented in WMPT unless the GSA is used.

It can be shown with some algebra (see appendix B) that with a Gaussian density  $\rho(x; \mu^*, \sigma^*)$  as in sections 3.1 and 3.2 the beam–beam kick is

$$K_{\text{yo}}[\rho](x) = \sqrt{\frac{\pi}{2}} \frac{\zeta}{\sigma^*} \Im W \left( \frac{x - \mu^*}{\sqrt{2}\sigma^*} \right) , \quad W(z) := e^{-z^2} \left( 1 + \frac{2i}{\sqrt{\pi}} \int_0^z e^{t^2} dt \right) , \quad z \in \mathbb{C} . \quad (3.37)$$

Here  $W$  is the complex “error” function [GR81] which is implemented for example in the CERNLIB [CL01]. And analogously to sections 3.1 and 3.2

$$\xi_{\text{yo}} = \frac{\zeta}{4\pi} \frac{\beta_0}{\sigma^{*2}} . \quad (3.38)$$

Note that in the YO limit the beam width  $\sigma^*$  appears squared in the denominator in contrast to the CR and the AS limit where it only appears linearly in the denominator. This is because the kernel has the dimension of  $q^{-1}$  in the YO case and the dimension of 1 in the CR and the AS cases.

In the last two sections we will *only* discuss the beam–beam interaction in the *pp*–case. Therefore  $\zeta$  and thus  $\xi_{\text{cr}}$ ,  $\xi_{\text{as}}$  and  $\xi_{\text{yo}}$  are negative by definition. Nevertheless we will for convenience redefine  $\xi$  in the *pp* case via  $Q = Q_0 - \xi + O(\kappa^2 \beta^2)$ , i.e.  $\xi \rightarrow -\xi$  !

## 4 Accuracy Considerations for WMPT

The primary error in the method comes from the computation of the kicks as discussed in section 2.2.1. As mentioned there, we are looking at simple models to try to obtain a feel for the optimal

$\Delta$  given  $\Theta$ . Wollman [WO96, WO99, WO00] has given a convergence proof for a 1-D model used in plasma physics to describe Coulomb-interacting electrons with a fixed ion background. Here we present some preliminary simulations which give us some confidence in the method before proceeding to the simulations of the  $\pi$  and the  $\sigma$  mode.

We first discuss the choice of the mesh size. We then discuss the evolution of the first four moments of  $q$  in the case where the two beams are identical and the initial distribution is an equilibrium of the linearized beam-beam force. Finally we discuss in Fig. 3 and 4 the particle distribution after  $2^{17} = 131072$  turns in a special case.

The discretization scale  $\Delta$  is (in principle for  $p$  and  $q$  independently) given by the initial mesh size divided by the number of macro-particles per dimension. Here and in section 5 we have chosen normalized coordinates ( $\beta_0 = 1 \Rightarrow \sigma_{q,0} = \sigma_{p,0} =: \sigma_0$ ), a square mesh from  $-5\sigma_0$  to  $+5\sigma_0$ , and between 51 ( $\Delta = 0.2\sigma_0$ ) and 401 ( $\Delta = 0.025\sigma_0$ ) macro-particles per phase space dimension, initially uniformly distributed on a square mesh for both beams. We cannot expect dynamics on a spatial scale which is much smaller than the discretization scale  $\Delta$  of the initial mesh to be visible during our simulations. In fact we should consider every effect that appears at a scale  $\ll \Delta$ , e.g. small amplitude fluctuations of the position of the beam centroid or of the square root of the beam emittance, as an artifact of the unavoidable discretization noise.

In the case of the linearized beam-beam force there are stationary densities in which each beam has the same density. Given a density such that  $\langle q \rangle = 0$  there is a  $\kappa$  defined by (2.5). This  $\kappa$  gives the perturbed betatron ellipses defined by (2.7c). It can be shown that there are densities whose equal density contours match the associated betatron ellipses. A special example for such a stationary solution of the linearized beam-beam force is the double Gaussian

$$\psi(\vec{z}) = \frac{1}{2\pi\sigma^2} e^{-\frac{1}{2}\vec{z}^T \underline{C}^{-1} \vec{z}} \quad , \quad \underline{C} := \begin{pmatrix} \beta & -\alpha \\ -\alpha & \gamma \end{pmatrix} \quad (4.39)$$

where the perturbed Courant-Snyder functions are given by (2.7c). This is discussed in some detail in [EW01]. It is also announced there that in the corresponding Vlasov-Fokker-Planck system (i.e. with the addition of damping and diffusion due to, for example, radiation) there exists a unique stationary solution. Numerical simulations suggest that this solution is stable for small current. It is not yet known if equilibria exist in the radiation free case nor if the equilibria are stable in the radiation free case with a linearized force. However, the results of WMPT below are consistent with an approximately stable density over  $2^{17}$  turns. This is also consistent with the behavior of actual beams in colliders which normally show only a slow emittance growth.

In the CR case which is so far the only one where WMPT can be done at less than  $O(N^2)$  *without* GSA we have studied the evolutions of a distribution that is stationary under the linearized beam-beam force. Using Eq. (2.7c) with  $Q_0 = \sqrt{5} - 2$ ,  $\xi = 3 \cdot 10^{-3}$ ,  $\beta_0 = 1$  and  $\alpha_0 = 0$  we find  $\beta \approx 1.0018$ ,  $\alpha \approx -0.0188$  and  $\gamma \approx 0.9985$  just after the kick. Note that this is still fairly close to the invariant circles of the unperturbed motion. We chose identical double Gaussians for each beam, given by (4.39). We simulate  $2^{17}$  turns with and without the Gaussian source approximation with  $n = 51, 101, 201, 401$  and with  $n = 51, 101$  and  $201$  macro-particles *per phase space dimension* respectively.

Fig. 2 shows the evolution of the centroid amplitude  $\langle q \rangle_{m2\pi}$  as a function of the number

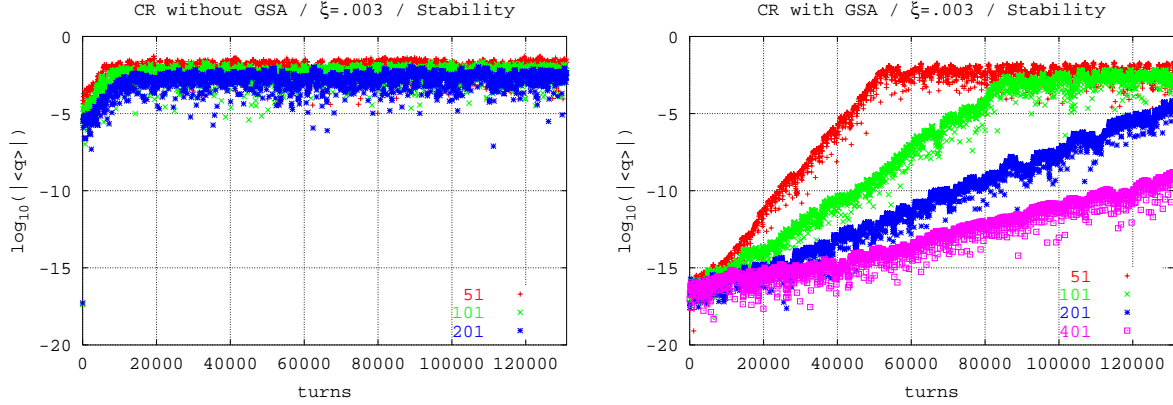


Figure 2: (color) The centroid position  $\langle q \rangle$  of the linearly matched phase space distribution with WMPT for the CR beam-beam force.  $\langle q \rangle$  is normalized by  $\sigma_0$ . Only each 64-th turn is actually printed. Left: “exact” ( $O(N \log N)$ ) computation of the beam-beam kick ( $n=51, 101$  and  $201$ ). Right: Gaussian source approximation ( $n=51, 101, 201$  and  $401$ ).

of turns  $m$ . The vertical scale is the logarithm to base 10 of  $\langle q \rangle_{m2\pi}$  in units of  $\sigma_0$  and the horizontal scale is  $m$ . All scatter plots start at around  $10^{-16}$  (DOUBLE PRECISION). With the “exact” computation of  $K_{\text{cr}}[\rho^*]$  (Fig. 2 left) the centroid amplitude immediately jumps to about  $10^{-5}$  and then exponentially (linearly in the logarithmic scale) grows until a saturation limit is reached. With the additional smoothing of the GSA (Fig. 2 right) the centroid amplitude grows exponentially from  $10^{-16}$  to a saturation limit.

The decrease in the saturation level with  $n$  seems to be significant and the saturation level itself is consistent with the size of  $\Delta$  under the assumption of a quasi-stationary state with  $\langle q \rangle = 0$ . The logarithmic slope of the envelope seems to be independent of  $n$  in the “exact” case whereas in the case of the GSA the logarithmic slope seems to be roughly proportional to  $n^{-3/4}$ . We do not understand this slope nor the jump from  $10^{-16}$  to  $10^{-5}$  in the “exact” case.

The 2-nd order centered moments and and therefore the beam emittance

$$\epsilon := \sqrt{\langle (q - \langle q \rangle)^2 \rangle \langle (p - \langle p \rangle)^2 \rangle - \langle (q - \langle q \rangle)(p - \langle p \rangle) \rangle^2} \quad (4.40)$$

stay constant on the 0.1–5% level (monotonically improving with decreasing discretization scale) in all simulations starting with a stationary Gaussian density of the linearized motion. The centered 4-th order moments are consistent with the assumption of a Gaussian beam (e.g.  $\langle (q - \mu_q)^4 \rangle_\theta = 3(\langle (q - \mu_q)^2 \rangle_\theta)^2$  with  $\mu_q = \langle q \rangle_\theta$ ) also on the level of a couple of percent.

The centered 3-th order moments oscillate around 0. Similar to the first order moments their oscillation amplitude grows exponentially with time until it saturates. The saturation level decreases with decreasing  $\Delta$ , but at a higher value then the level for  $\langle q \rangle$ . Note that for a Gaussian distribution, as for any distribution whose density is even around its mean, all odd centered moments vanish identically. Thus the relatively high saturation level of the third order moments, suggests that the GSA should be revised and a different test density which allows odd centered moments should be used in (2.23).

Force	$\Delta/\sigma_0$	$\max  \langle q \rangle /\sigma_0$	$\max  1 - \epsilon/\sigma_0^2 $	$\max  \langle (q - \langle q \rangle)^3 \rangle/\sigma_0^3 $
CR	0.200	0.06	0.05	0.2
	0.100	0.025	0.015	0.1
	0.050	0.01	0.001	0.05
CR/GSA	0.200	0.025	0.004	0.2
	0.100	0.008	0.0008	0.1
	0.050	No saturation in $2^{17}$ turns		
	0.025			
AS/GSA	0.200	0.05	0.0025	0.25
	0.100	0.02	0.001	0.12
	0.050	0.007	0.0005	0.04
YO/GSA	0.200	0.06	0.01	0.4
	0.100	0.015	0.002	0.1
	0.050	0.006	0.0004	0.04

Table 1: The approximate bounds of  $\langle q \rangle$  and  $\langle (q - \langle q \rangle)^3 \rangle$  and the approximate maximum deviation of the emittance from  $\sigma_0^2$  for the 4 model forces under numerical study.  $\Delta$  is the grid spacing.

In all simulations discussed so far the agreement between  $\langle q^v p^w \rangle_\theta$  and  $\langle q^v p^w \rangle_\theta^*$  was better than  $10^{-4}$  which is not surprising for a evolution equation being symmetric under  $\psi \leftrightarrow \psi^*$  and identical initial conditions for both beams.

Similar simulations exist for the AS and the YO beam–beam limits, both in the Gaussian Source approximation, and they show qualitatively the same stability properties as the case of the CR interaction. Moreover they give quantitatively similar results concerning saturation amplitudes and logarithmic slopes. The approximate saturation levels of the fluctuations of the 1-st and 3-rd moments as well as the fluctuations in the beam emittance are shown in Tab. 1.

The numerical simulations shown in Fig. 2 and Tab. 1 not only give some confidence in WMPT but also seem to indicate the existence of at least quasi-stationary phase space densities under the full nonlinear collective beam–beam interaction in 1-D.

Since in the WMPT approach the phase space integrals in the expectation values  $\langle f \rangle_\theta$  and in the beam–beam kicks  $K[\rho_{\theta_c}^*]$  are approximated by sums over the trajectories  $\vec{\eta}_{ij}$  and  $\vec{\eta}_{ij}^*$  respectively, it has to be checked whether or not the effective distribution of the trajectories leads to a sufficiently slowly varying coarse grained density in the sense of (2.18) or not. Although “spikes” and “holes” in the coarse grained density might as well be of physical origin, one might expect that the numerical accuracy of the numerical representation of the phase space integral suffers if the coarse grained density is too rapidly varying.

Fig. 3 (left) shows a scatter plot of all the trajectories of one beam after  $2^{17}$  turns. The initial mesh was set up identically to the simulations for Fig. 2 with  $201 \times 201$  macro-particles per beam but the beams were initially exactly round (in the normalized coordinates) and the “other” beam (not shown) had an initial offset of  $0.1\sigma_0$ . Again the beam–beam tune shift parameter was

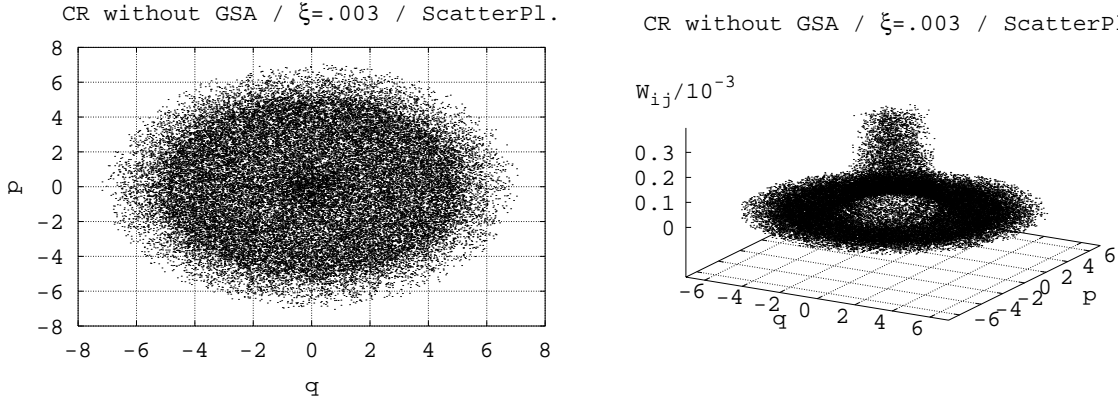


Figure 3: Scatter plots of  $\vec{\eta}_{ij}(\theta)$  (left) and  $(\vec{\eta}_{ij}(\theta), \mathfrak{W}_{ij})$  after  $2^{17}$  turns.  $q$  and  $p$  are normalized by  $\sigma_0$ .

chosen to be  $3 \cdot 10^{-3}$ . The unperturbed tunes were  $Q_0^* = \sqrt{5} - 2$  and  $Q_0 = Q_0^* - 5 \cdot 10^{-6}$ . Therefore the beams are expected to be collectively coupled [AL99, CR85, YK90, YZ93, HO99, ZZ99] and indeed in section 5 the existence of a  $\pi$ - and a  $\sigma$ -mode will be demonstrated. Note that for non-vanishing beam-beam tune shift parameter, the beams are of course coupled for all tunes. The phrase “coupled” is used in the literature to describe the situation that for equal unperturbed tunes the  $\pi$  and  $\sigma$  modes are most prominent. In the rigid bunch model of Hofmann [HO99] the  $\pi$  and  $\sigma$  modes are eigenmodes for equal tunes but not for unequal tunes. We will discuss this in more detail in section 5.

With these maximally “coupled” beams ( $|Q_0 - Q_0^*| \ll \xi$ ) one expects the strongest distortions of the phase space distributions. Nevertheless it has to be noted that in all simulations, performed for this study so far, the unperturbed tunes were chosen *far* away from all lower order resonances of the single particle motion. Simulations close to resonances have to be made in the near future.

Thus the particles with the largest initial offset The scatter plot in Fig. 3 (left) shows the distribution of the trajectories in the phase plane after  $2^{17}$  turns. Note that the initial mesh was square from  $-5$  to  $+5\sigma_0$  in both phase space dimensions. Thus the particles with the largest initial offset are at a distance of  $(\sqrt{5^2 + 5^2} \approx 7)\sigma_0$  from the center. The distribution appears uniform except for a halo-like ring of reduced point density. The appearance of this halo-like ring from about  $5\sigma_0$  to about  $7\sigma_0$  is most likely an artifact of the square initial mesh. We thus conclude that the macro particles remain uniformly distributed in a coarse grained sense.

Fig. 3 (right) shows a 3-D scatter plot of the macro-particle weights  $\mathfrak{W}_{ij} = \psi_0(\vec{z}_{ij})w_{ij}$  over the actual position of the trajectory  $\vec{\eta}_{ij}(\theta)$  after  $2^{17} = 131072$  turns. Since in the current implementation of the algorithm  $w_{ij} = w = \text{const.}$  and since the initial density was a round centered Gaussian, the vertical coordinate of each point is a measure for the initial distance from the origin:  $\sqrt{q_i^2 + p_j^2} = \sqrt{-2 \ln(2\pi\psi_0(\vec{z}_{ij}))}$ . Obviously the majority of particles that initially belonged to the core stay relatively close to the core. Otherwise the scatter plot would

look less like a “bell” and look more like a uniform cloud.

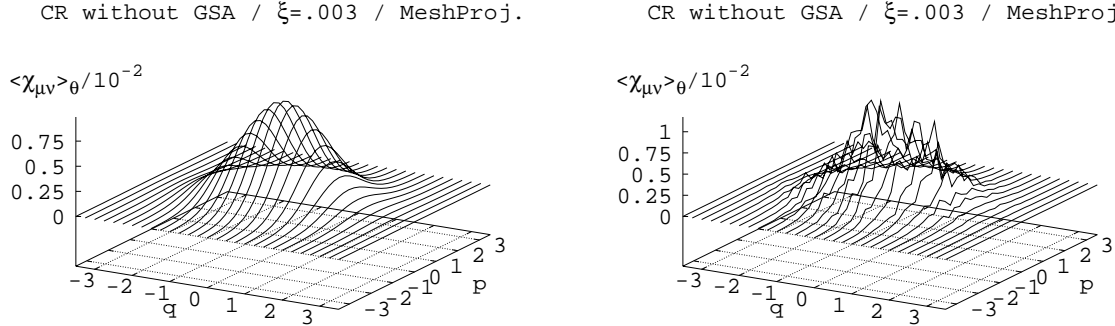


Figure 4: Mesh projections  $\langle \chi_{\mu\nu} \rangle_\theta$  after 0 turns (= initial data) (left) and after  $2^{17}$  turns (right). The mesh that  $\psi_\theta$  was projected on was in both cases given by  $41 \times 41$  mesh points from  $-5$  to  $+5\sigma_0$  and the initial mesh of the macro-particles had  $201 \times 201$  point in the same range.  $q$  and  $p$  are normalized by  $\sigma_0$ . To emphasize shape of the core only the range from  $-3.5$  to  $+3.5\sigma_0$  is shown

Fig. 4 shows projections of  $\psi_\theta$  (2.18) on a mesh of  $41 \times 41$  mesh points for the initial Gaussian (left) and after  $2^{17}$  turns (right). The parameters of the simulation were the same as for Fig. 3.<sup>2</sup> A scatter plot of the *initial* data would of course coincide with the surface of Fig. 4 (left). But after  $2^{17}$  turns the scatter plot 3 (right) is a diffuse bell-shaped cloud and the coarse grained mesh projection gives an indication of the actual density. The mesh-projection of Fig. 4 (right) looks a little jagged. This is due in part to the particular choice of the partition of unity in this mesh-projection. This is also due in part to the dynamics which can bring two initially separated particles, with significantly different densities, close together. However, the mesh projection has a well defined core and each of the core bins has a significant amount of probability assigned to it. Moreover the projected density at the edge of the core decreases relatively smoothly and there are no islands outside the core. The coarse grained density as obtained by  $2^{17}$  turns of WMPT therefore has a slowly varying component (the bell) and a rapidly varying component (the peaks and valleys). In phase space averages the slowly varying part will be represented with relative high accuracy and the the rapidly varying part, which contributes only little to the average, will be represented with relatively low accuracy.

The actual smoothness of the mesh-projection depends on the coarseness of the mesh and of the smoothing effect of the partitioning of unity chosen. The indicator functions  $\chi_{\mu\nu}$  are the simplest ones but they also are those with the least smoothing. Projecting on a mesh with  $21 \times 21$  points produces a much smoother surface and increasing the number of mesh points to  $81 \times 81$  yields a projection with numerous spikes inside the core region of Fig. 4 (right).

Since WMPT is designed to compute *integrals* including the density rather than computing the density itself, we have gained confidence that the “smoothness” observed in the presented example, together with the apparent convergence in  $\Delta$  observed in Tab. 1 and Fig. 2 seems

<sup>2</sup>Actually it was the same run. BBDemo1D comes with various post-processing facilities.

sufficient to provide a relatively accurate time evolution of the low order moments on scales well above the discretization scale and for a finite number of turns.

It must be noted that a completely mesh based method, like the PF method, always gives an approximation of  $\psi_\theta$  on the fixed mesh and does not require coarsening.

## 5 Simulations

One key task of this stage of the study was to identify the  $\pi$ - and  $\sigma$ -modes for the Three different 1-D limits of the beam-beam force and to discuss their dependence on the difference of the unperturbed tunes  $\Delta Q := Q_0 - Q_0^*$  and  $\Delta \xi := \xi - \xi^*$ . Moreover the onset of Landau-damping for  $\Delta Q > \xi$  should be observable.

We have performed a large number of simulation runs with different parameter sets and only a fraction of them can be presented here.

For comparison we will use a trivial extension of the rigid bunch model described in [HO99]. Under the assumption of rigid bunches and a linearized beam-beam force the motion the beam centroids  $X := \langle q \rangle$  and  $X^* := \langle q \rangle^*$  is equivalent to a system of two coupled linear oscillators

$$\frac{d^2}{d\theta^2} X + (Q_0^2 + Q_0 \xi) X - Q_0 \xi X^* = 0 \quad (5.41a)$$

$$\frac{d^2}{d\theta^2} X^* + (Q_0^{*2} + Q_0^* \xi^*) X^* - Q_0^* \xi^* X = 0 \quad (5.41b)$$

The eigentunes  $Q^+$  and  $Q^-$  are easily found to be

$$(Q^\pm)^2 = \frac{1}{2} \left( Q_0^2 + Q_0^{*2} + Q_0 \xi + Q_0^* \xi^* \mp \text{sgn}(\xi) \sqrt{(Q_0^2 - Q_0^{*2})^2 + (Q_0 \xi + Q_0^* \xi^*)^2 + 2(Q_0^2(Q_0 \xi - Q_0^* \xi^*) + Q_0^{*2}(Q_0^* \xi^* - Q_0 \xi))} \right). \quad (5.42)$$

In the case of  $\xi^* = \xi$  this reproduces the result presented in [HO99]

$$(Q^\pm)^2 = \frac{1}{2} \left( Q_0^2 + Q_0^{*2} + \xi(Q_0 + Q_0^*) \mp \text{sgn}(\xi) \sqrt{(Q_0^2 - Q_0^{*2})^2 + \xi^2(Q_0 + Q_0^*)^2 + 2\xi((Q_0 + Q_0^*)(Q_0 - Q_0^*)^2)} \right). \quad (5.43)$$

For  $Q_0^* = Q_0$  we find

$$(Q^\pm)^2 = Q_0^2 + Q_0 \frac{\xi + \xi^*}{2} \mp \text{sgn}(\xi) \left| Q_0 \frac{\xi + \xi^*}{2} \right|, \quad (5.44)$$

and for simultaneously  $\xi^* = \xi$  and  $Q_0^* = Q_0$

$$(Q^\pm)^2 = Q_0^2 + Q_0 \xi \mp \text{sgn}(\xi) |Q_0 \xi| \Rightarrow \left. \begin{matrix} Q^+ \\ Q^- \end{matrix} \right\} \xrightarrow{|\xi| \ll Q_0} \begin{cases} Q_0 \\ Q_0 + \xi \end{cases}. \quad (5.45)$$

It was shown in [HO99] that in this last case the eigenmodes to  $Q^+$  and  $Q^-$  correspond to the  $\sigma$ -mode ( $X + X^*$ ) and the  $\pi$ -mode ( $X - X^*$ ). It is not surprising that in this simple model the  $\pi$ -mode frequency for  $|\xi| \ll Q_0$  does not contain the Yokoya factor  $Y$  ( $Q_\pi = Q + Y\xi$ ) which was predicted to differ from 1 in [YK90] by means of the linear Vlasov theory. Note that for  $Q_0^* \neq Q_0$  the  $\pi$ -mode and the  $\sigma$ -mode are *not* the eigenmodes even of the rigid bunch model.

In the following we will discuss the spectra obtained by simulations using WMPT and the onset of damping of the modes and compare the the most prominent frequencies of the spectra with the eigentunes  $Q^+$  and  $Q^-$  of the rigid bunch model.

### 5.1 The dependence of the $\pi$ and $\sigma$ modes on $\Delta Q$

In this section we will present results of simulations in the three cases: CR *without* GSA in Fig. 5, AS with GSA in Fig. 6 and YO with GSA in Fig. 7. The parameter sets will be basically identical. In particular the beam-beam tune shift parameter is the same ( $|\xi| = 3 \cdot 10^{-3}$ ) for all simulations in this section. The figures are structured as follows: The first three plots are tune

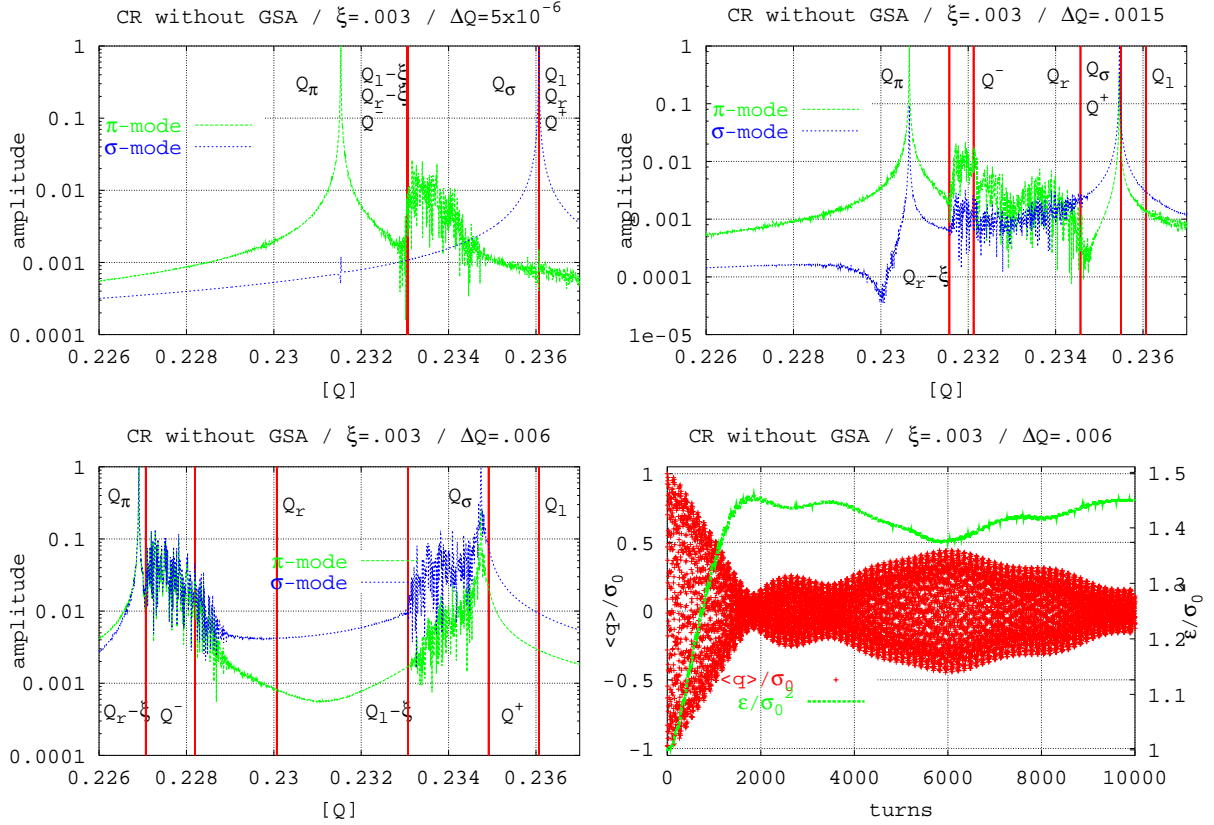


Figure 5: (color) Chao-Ruth limit: FFT analysis of the  $\pi$ - and  $\sigma$ -mode for  $\Delta Q = 5 \cdot 10^{-6}$ ,  $1.5 \cdot 10^{-3}$  and  $6.0 \cdot 10^{-3}$  (clockwise top left to bottom left). Bottom right: time evolution of  $\langle q_i \rangle$  and  $\epsilon_i$  for the first 10,000 turns.

spectra, i.e. the modulus of the Fourier amplitude computed by a FFT based on  $2^{17}$  turns, for the  $\pi$ -mode  $\langle q \rangle - \langle q \rangle^*$  (light/green) and the  $\sigma$ -mode  $\langle q \rangle + \langle q \rangle^*$  (dark/blue).<sup>3</sup> The spectra are normalized so that the largest amplitude is 1. The thick vertical (red) lines (cursors) that appear in all spectra are markers e.g.  $Q_l$ ,  $Q_r$ ,  $Q_l - |\xi|$ ,  $Q_r - |\xi|$ ,  $Q^+$ , and  $Q^-$ . The initial conditions for the simulations used to compute the spectra are round Gaussians, i.e. Gaussians matched to the unperturbed optics in normalized coordinates, with  $\sigma_0 = 1$  for both beams, one beam (R) being initially centered around the origin and the other beam (L) having an initial  $q$ -offset of  $0.1\sigma_0$ . The unperturbed tune of beam L was always set to  $Q_l := \sqrt{5} - 2 \approx 0.23606798$  and the unperturbed tune of beam R was set to  $Q_r := Q_l - 5 \cdot 10^{-6}$ ,  $1.5 \cdot 10^{-3}$  or  $6 \cdot 10^{-3}$  for the top left, top right and bottom left plot respectively. The only exception is the YO case (Fig. 7) where, because of reasons to be explained later, the top right plot has a  $\Delta Q$  of  $0.5 \cdot 10^{-3}$  instead of  $1.5 \cdot 10^{-3}$ . In all cases the bottom right plot shows the time evolution of  $\langle q_l \rangle$  and the beam emittance of beam L for the first  $10^4$  turns and for  $\Delta Q = 6 \cdot 10^{-3}$ . There the initial offset of beam L was  $1.0\sigma_0$ .

The viewpoint for all simulations is  $\theta_c^+$ , i.e. the position directly *after* the IP and the initial mesh has  $201 \times 201$  points uniformly distributed on rectangle in phase space from  $-5$  to  $+5\sigma_0$ .

Since the CR limit is the only one where a reasonably fast ( $O(N \log N)$ ) algorithm for the computation of the beam-beam kick *without* the additional simplification of the Gaussian source approximation has yet been found, Fig. 5 is the only one which shows the results of simulations with the “exact” WMPT. In Fig. 5 (top left) the unperturbed tunes are so close together ( $\Delta Q = 5 \cdot 10^{-6} \Rightarrow Q_r \approx Q_l =: Q_0 \approx Q^+$ ) that they can not be distinguished on the chosen scale. The main and clearly visible features in 5 (top left) are the  $\pi$  and  $\sigma$ -modes and the noisy continuum. The continuum originates from the single particle motion. It reflects the incoherent tune spread and falls off sharply at  $Q_0 - |\xi|$ . In addition it goes strongly to zero as  $Q \rightarrow Q_0$ . In the weak-strong approximation (and for  $pp$  collisions) the weak beam has an amplitude dependent tune spread from  $Q_0$  at infinitely large amplitude to  $Q_0 - |\xi|$  at zero amplitude. Since the initial phase space mesh has a cut-off at  $\pm 5\sigma_0$  and since the outermost macro-particles carry a basically vanishing weight, the amplitude of the continuum decreases strongly as  $Q \rightarrow Q_0$ . The  $\sigma$ -mode (blue) has a sharp peak at  $Q_0$  as expected by the theory [CR85, YK90, YZ93, AL99, HO99]. The position of the peak amplitude of the  $\pi$ -mode (green) at  $0.231537 \approx Q_0 - 1.51|\xi|$ . The linearized Vlasov theory predicts that the  $\pi$ -mode should emerge from the continuum, but numerical estimates for the CR force with an initial Gaussian density have to our knowledge not been published. Note that the  $\sigma$ -mode has a small peak at the major peak of the  $\pi$ -mode. Moreover, the  $\pi$ -mode contains the continuum whereas the  $\sigma$ -mode does not. This is a peculiarity of the CR force and we do not have an explanation yet.

Fig. 5 (top right) shows the spectrum with  $\Delta Q = |\xi|/2$ . Very close to  $Q^+$ , at  $0.23545$  lies the most prominent peak of the  $\sigma$ -mode. Now both the  $\sigma$ - and the  $\pi$ -mode show a continuum that ends at  $Q_r - |\xi|$ . The envelope of the continuum in the  $\pi$ -mode spectrum has a visible minimum at  $Q_l - |\xi|$  (*no* cursor). The largest peak of the  $\pi$  mode is at a distance of  $1.61|\xi|$  left

---

<sup>3</sup>In the printed black-and-white version the green curves appear relatively light and the blue curves appear relatively dark. Since we're in the 21-st century, we will put this report on the web (in color of course) and will identify the curves by their color and *not* by their darkness.

of the largest peak of the  $\sigma$ -mode. We note that the  $\pi$  and  $\sigma$  modes are not the eigenmodes of the linearized motion when  $\Delta Q \neq 0$ . In fact both modes have *two* prominent peaks at the same position. As we will see later, this is true for all three forces. Nevertheless, as long as  $\Delta Q \ll |\xi|$ , the largest peak of the  $\sigma$  mode always between  $Q_l$  and  $Q_r$  and the largest peak of the  $\pi$ -mode is always left of the continuum.

The envelopes of  $\langle q \rangle_\theta \pm \langle q \rangle_\theta^*$  and the beam emittances, which are *not* shown here, are in both cases ( $\Delta Q = 5 \cdot 10^{-6}$  and  $1.5 \cdot 10^{-3}$ ) basically constant and neither show significant damping of the centroid motion nor emittance blow-up up to 130000 turns. This situation changes when  $\Delta Q = 2|\xi|$  (bottom two plots of Fig. 5). Note that both spectra have a strong peak close to  $Q^+$ . Moreover the continuum now has two disjoint parts. One continuum ranges from  $Q_l - |\xi|$  to  $Q^+$ . The second part of the continuum ranges from about  $Q_r - 0.4|\xi|$  to  $Q_r - |\xi|$  and slightly left of the continuum at 0.22691 lies the second strong peak of both the  $\pi$  and the  $\sigma$  mode. The two peaks are separated by  $2.61|\xi|$ . The strongest peak in both spectra is a little left of the  $Q_r - |\xi|$ . We conclude that with this tune separation the characteristic separation of the main peak of both modes disappears. Nevertheless with the CR force even at  $\Delta Q = 2|\xi|$  there are still 2 distinct main peaks in the spectra. We will see that with the AS and the YO force at this tune separation the two prominent peaks that correspond to the eigenmodes of the linearized Vlasov equation have already disappeared. Fig. 5 (bottom right) depicts another key difference to the cases with  $\Delta Q \ll |\xi|$ . The amplitude (red/dark points) of the centroid motion of the initially excited beam (L) decays with increasing revolution number on a scale larger but comparable to  $1/|\xi|$ . The emittance  $\epsilon_l$  (green/light line) grows on the same “time” scale from initially  $1\sigma_0^2$  to inbetween 1.4 and  $1.5\sigma_0^2$ . These effects indicate the onset of the so-called Landau-damping and is predicted by the linearized Vlasov theory [YK90, YZ93, AL99] for  $\Delta Q \gg |\xi|$ . Note that the centroid amplitude is not damped to 0 or at least to  $\Delta = 0.05\sigma_0$  but fluctuates between 0.1 and  $0.5\sigma_0$ . Comparing with Fig. 6 and 7 for the AS and the YO limit respectively we see that there the Landau-damping process leads to a much smaller stationary amplitude and a much more stable beam emittance. It is not yet clear whether this difference between CR on the one hand and AS and YO on the other hand has a physical meaning or whether it is an artifact of the algorithm. However, in a simulation with identical parameters and initial condition but using the Gaussian source approximation for the CR interaction (*not* shown) the effect of Fig. 5 was qualitatively reproduced.

Fig. 6 shows a qualitatively similar situation for the AS interaction as in Fig. 5. Both plots on the top show clearly separated  $\pi$ - and  $\sigma$ -modes. With  $\Delta Q = 5 \cdot 10^{-6}$ , i.e.  $Q_r \approx Q_l \equiv Q_0 \approx Q^+$  the  $\sigma$ -mode has its dominant peak at  $Q_0$  and the single particle continuum, which is now visible in both modes, has a sharp boundary at  $Q_0 - |\xi| \approx Q^-$ . The  $\pi$ -mode appears at about  $Q_0 - 1.27|\xi|$ . Relative to the CR case it is therefore shifted towards the  $\sigma$ -mode (and the continuum). In a similar simulation *without* GSA but only with  $75 \times 75$  macro-particles<sup>4</sup> the  $\pi$ -mode peak which was much more noisy was even shifted a little further ( $Q_0 - 1.25|\xi|$ ) towards the  $\sigma$ -mode. This case can be compared to the predictions of the linearized Vlasov theory [YK90, YZ93] and to the 2-D simulations recently performed by Zorzano and Zimmermann [ZZ99]. The linearized Vlasov

---

<sup>4</sup>On a modern Sun Ultra-80, BBDemo1D runs in the AS-mode 4.5h for  $201 \times 201$  particles *with* GSA and 120h for  $75 \times 75$  *without* GSA!

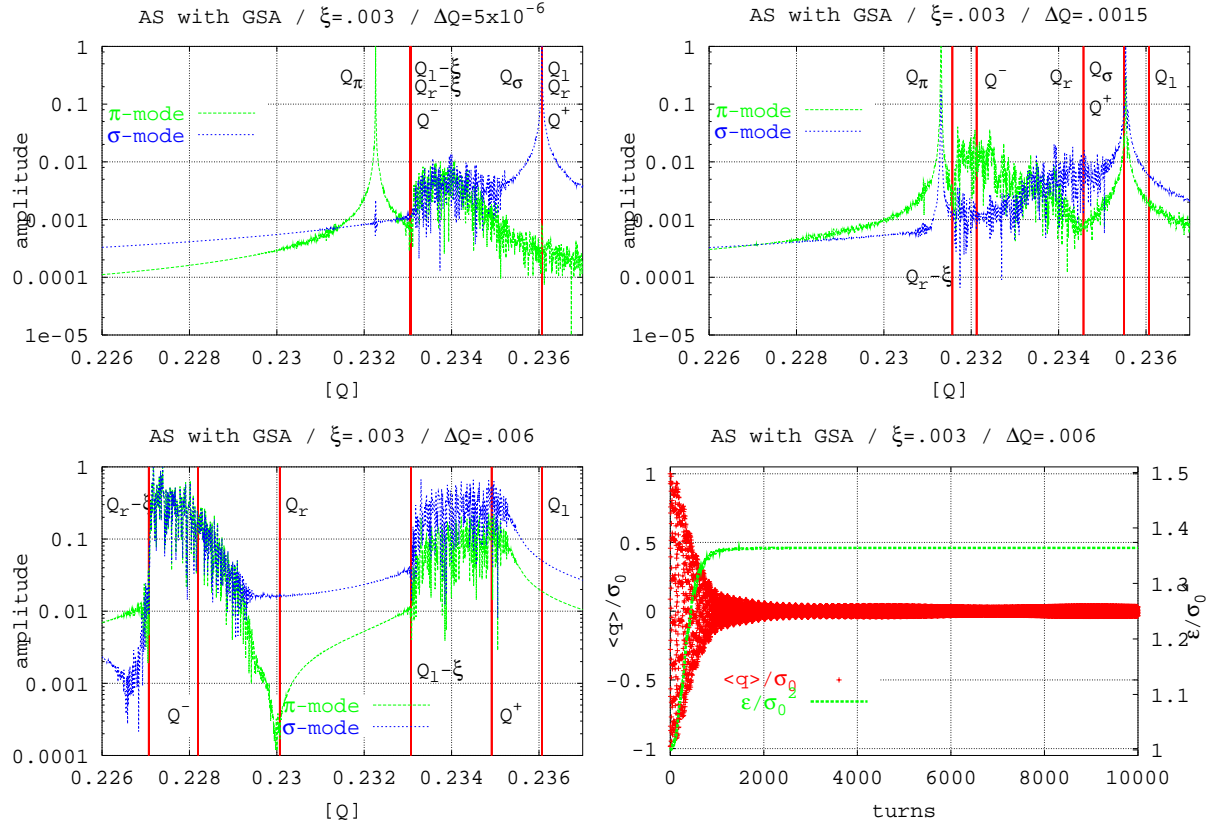


Figure 6: (color) Axially symmetric limit: FFT analysis of the  $\pi$ - and  $\sigma$ -mode for  $\Delta Q = 5 \cdot 10^{-6}$ ,  $1.5 \cdot 10^{-3}$  and  $6.0 \cdot 10^{-3}$  (clockwise top left to bottom left). Bottom right: time evolution of  $\langle q_i \rangle$  and  $\epsilon_i$  for the first 10,000 turns.

theory predicts the separation of  $\pi$ - and  $\sigma$ -modes of about  $1.21|\xi|$  and the 2-D simulations with an initially round beam represented by  $10^4$  non-weighted macro-particles performed in [ZZ99] yields a separation of about  $1.10|\xi|$ . At this stage it is not possible to argue whether or not the linearized Vlasov theory gives a more complete picture than nonlinear tracking studies using macro-particles and whether the full 2-D treatment in [ZZ99] compensates for their much smaller number of macro-particles per phase space dimension. So it is just fair to say that the 3 values for the separation of the two collective dipole modes, namely  $1.21|\xi|$ ,  $1.27|\xi|$  and  $1.10|\xi|$  are consistent with one-another.

In the top right plot of Fig. 6 with  $\Delta Q = 1.5 \cdot 10^{-3} = |\xi|/2$  we see that the  $\sigma$ -mode has its major peak close to  $Q^+$  in between  $Q_l$  and  $Q_r$ . The position of the  $\sigma$ -mode peak is basically the same as compared the CR interaction, but slightly shifted from  $Q^+$  towards the right. The  $\pi$ -mode appears at  $Q_\sigma - 1.41|\xi|$  but is already very close to the boundary of the single particle continuum at the leftmost cursor  $Q_r - |\xi|$ .

Fig. 6 (bottom left) with  $\Delta Q = 2|\xi|$  does not show any prominent singular peak in either spectra. The absence of any dominant frequencies in the spectra suggests that the motion of

the two centroids is basically “decoupled” (in the sense explained in section 4). The plot at the bottom right of Fig. 6 supports this result. The amplitude of the initially excited beam is Landau-damped to the discretization scale of the simulation. Note that in comparison with the CR limit the oscillation once damped into the noise level appears stationary. Also the beam emittance appears to be stable at about  $1.37\sigma_0^2$ .

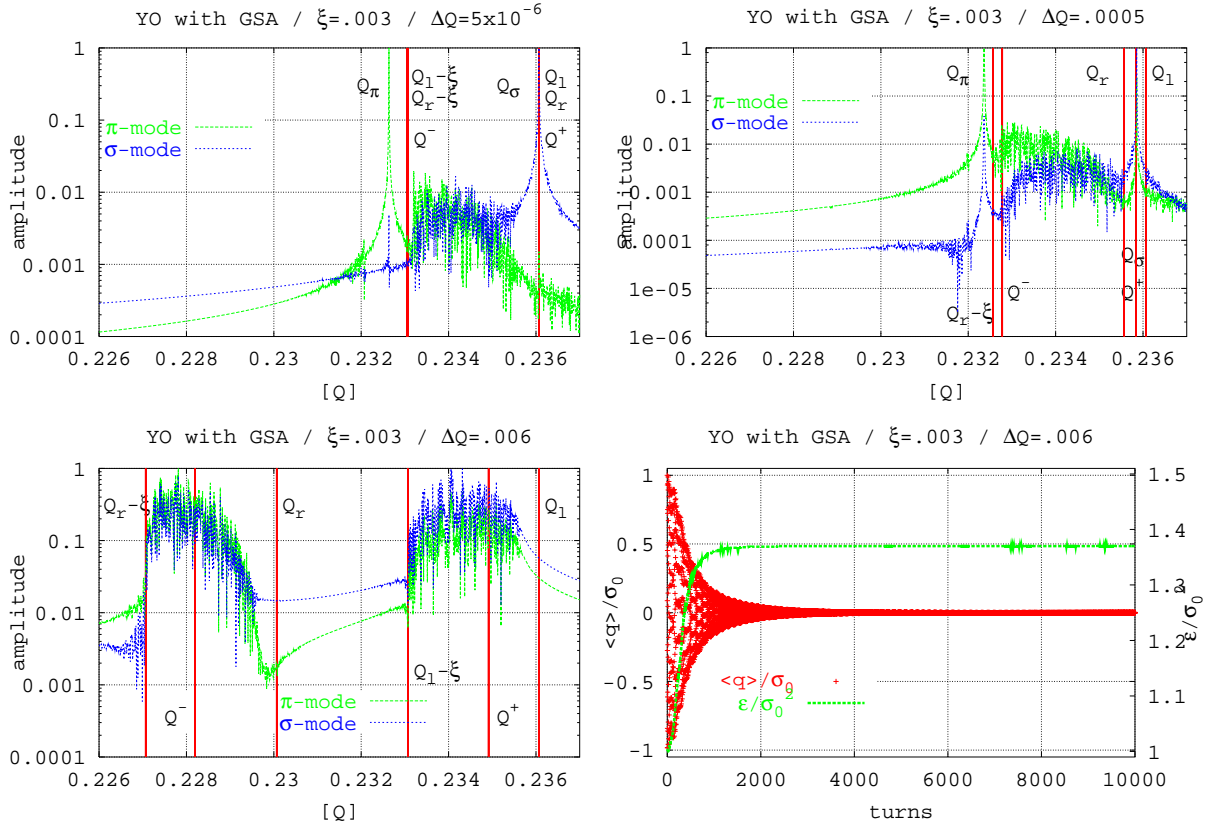


Figure 7: (color) Yokoya–Koiso–Zenkevich limit: FFT analysis of the  $\pi$ - and  $\sigma$ -mode for  $\Delta Q = 5 \cdot 10^{-6}$ ,  $0.5 \cdot 10^{-3}$  and  $6.0 \cdot 10^{-3}$  (clockwise top left to bottom left). Bottom right: time evolution of  $\langle q \rangle$  and  $\epsilon_l$  for the first 10,000 turns.

Fig. 7 shows the equivalent simulations for the YO limit. As we can easily see in the top left plot, the  $\pi$ -mode is now separated by  $1.14|\xi|$  from the  $\sigma$ -mode and thus even closer to the continuum. This again can be compared to the linear Vlasov theory applied in [YK90, YZ93] and the case of a “flat” beam (where “flat” means  $\sigma_x/\sigma_y = 16$ ) studied numerically in [ZZ99]. Yokoya & Koiso predict  $1.33|\xi|$  and Zorzano & Zimmerman find 1.15. Again we have to be aware that a quantitative comparison of the three methods is not really possible at this stage, but then again all three values are mainly consistent. Since the  $\pi$ -mode is so close to the continuum already with  $\Delta Q \ll |\xi|$ , it is no big surprise that with  $\Delta Q = |\xi|/2$  (*not shown*) the system is in a Landau-damped regime. In this case the amplitude of the centroid motion is damped to some intermediate value and the spectra show no *clear* signature of well defined  $\pi$  and  $\sigma$  modes.

Therefore Fig. 7 (top right) shows the spectra of the  $\pi$ - and  $\sigma$ -mode for  $\Delta Q = 0.5 \cdot 10^{-3}$  instead of  $1.5 \cdot 10^{-3}$  as in the CR and the AS case. Here the  $\pi$ -mode is about  $1.17|\xi|$  separated from the  $\sigma$ -mode. For comparison, the rigid bunch model predicts  $Q^+ = 0.23584$  (2-nd rightmost cursor) and  $Q^- = 0.23278$  (2-nd leftmost cursor). Note that in this example the continuum ends at  $Q^-$  rather than at  $Q_r - |\xi|$ . When  $\Delta Q$  is increased to  $6 \cdot 10^{-3}$  (bottom two plots), similar to the AS limit, the beams centroid motions are more or less completely decoupled and the initial amplitude of beam L is quickly damped to a value below the discretization scale.

It is worthwhile noting that in all our simulations the tune of the  $\sigma$ -mode basically coincides with  $Q^+$  obtained by means of the rigid bunch model, whereas the  $\pi$ -mode doesn't.

## 5.2 The dependence of the $\pi$ and $\sigma$ modes on $\Delta\xi$

It has been suggested in [AL99] that the  $\pi$ -mode moves back into the continuum when the ratio  $\xi/\xi^*$  is reduced to less than 0.6. In this section we briefly discuss our results in the three 1-D cases. Fig. 8 contains spectra of the  $\pi$  (light/green) and  $\sigma$  mode (dark/blue) for  $\xi_r/\xi_l = 0.6$  (left column) and 0.1667 (right column) and for CR (top row), AS with GSA (center row) and YO with GSA (bottom row). Both unperturbed tunes were chosen identical  $Q_l = Q_r = \sqrt{5} - 2$  and the left beam had an initial  $q$ -offset of  $0.1\sigma_0$ .  $\xi_l = -0.003$  was kept constant and  $\xi_r$  was varied. The thick red cursors mark  $Q^+ = \sqrt{5} - 2$  (left) and  $Q^-$  (right).  $Q^-$  is 0.23366 when  $\xi_r/\xi_l = 0.6$  and 0.23431 when  $\xi_r/\xi_l = 0.1667$ .

It is easy to see that in all six plots the  $\sigma$ -mode has its most pronounced peak at  $Q^+$ . Moreover, if  $\xi_r/\xi_l = 0.1667$  then the  $\pi$ -mode peak has either disappeared completely (AS and YO) or is just a noisy maximum at the edge of the continuum (CR). In all three cases, the initial excitation is damped, accompanied by a slight emittance growth. When  $\xi_r/\xi_l = 0.6$ , the separations of the  $\pi$  and the  $\sigma$ -mode are  $1.52|\xi_l + \xi_r|/2$ ,  $1.30|\xi_l + \xi_r|/2$  and  $1.19|\xi_l + \xi_r|/2$  for CR, AS and YO respectively. With this ratio of the beam-beam parameters little or no damping was observed. The intensity ratio at which the  $\pi$ -mode just emerges from the continuum therefore depends on the model of the force.

Again we note that in all our simulations the tune of the  $\sigma$ -mode basically coincides with  $Q^+$  obtained by means of the rigid bunch model, whereas the  $\pi$ -mode doesn't.

## 6 Conclusion and Outlook

We have studied the strong-strong beam-beam interaction by means of a method for simulating the evolution of the moments of the phase space distribution under collective Hamiltonian forces following the VE. This method, WMPPT, has been implemented in a code for simulations BBDemo1D.

Three different limits, the Chao-Ruth, the axially symmetric and the Yokoya-Koiso-Zenkevich, have been studied numerically. The results are qualitatively consistent with the linearized Vlasov theory as well as with simulations performed by other groups, although they suggest small quantitative corrections to the results of the linearized theory.

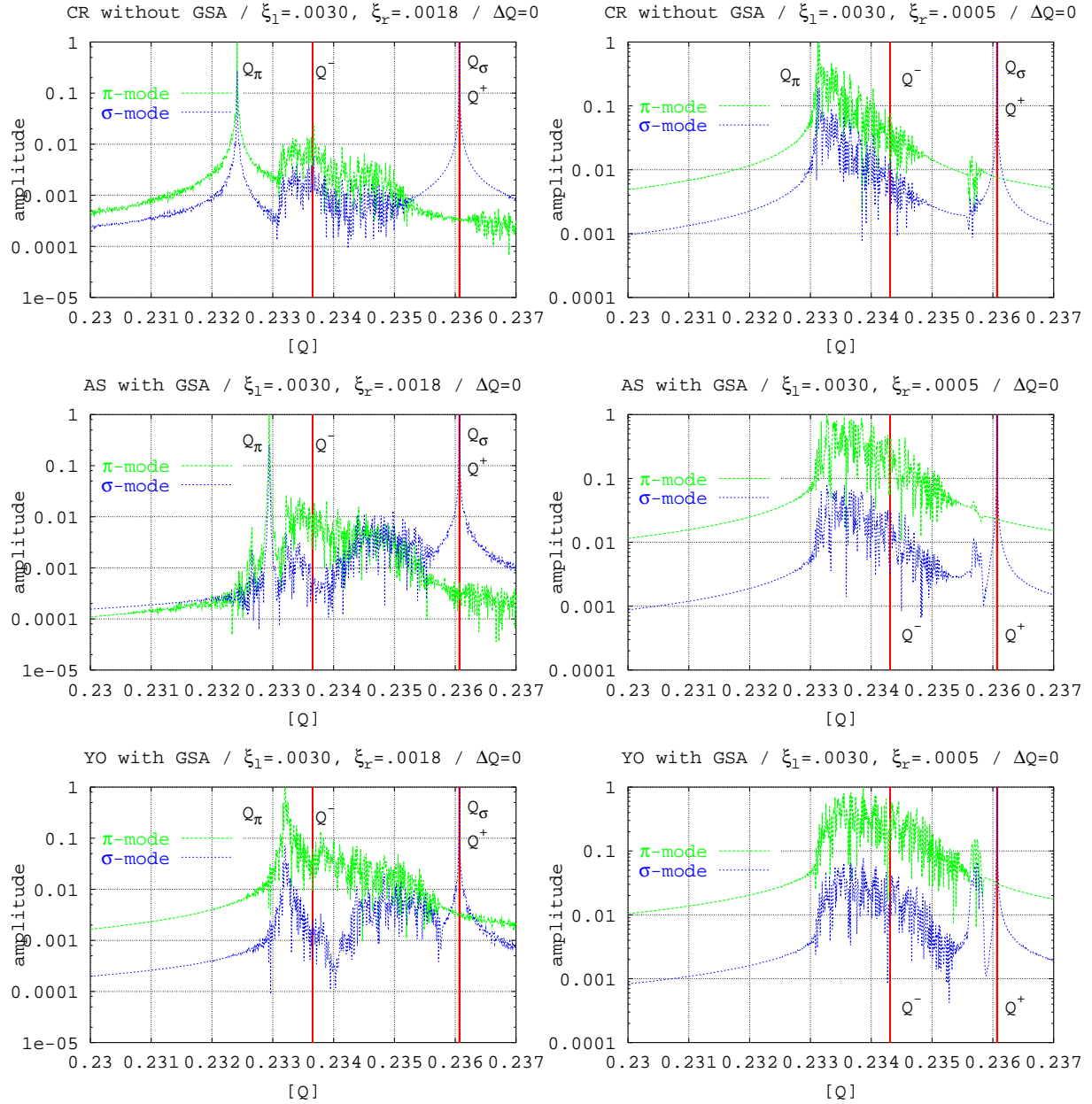


Figure 8: (color) FFT analysis of the  $\pi$ - and  $\sigma$ -mode for  $\xi_r/\xi_l = 0.6$  (left) and  $0.1667$  (right). Top row: CR; center row: AS; bottom row: YO.

Force	$\Delta Q$	$\xi_r$	$Q_\sigma - Q_\pi$	Damping
CR	0	$0.6\xi_l$	$1.52(\xi_l + \xi_r)/2$	no
	0	$0.1667\xi_l$	$(1.67(\xi_l + \xi_r)/2)^\dagger$	yes
	$5 \cdot 10^{-6}$	$\xi_l$	$1.51\xi$	no
	$1.5 \cdot 10^{-3}$	$\xi_l$	$1.60\xi$	no
	$6.0 \cdot 10^{-3}$	$\xi_l$	$(2.61\xi)^\dagger$	yes
AS/GSA	0	$0.6\xi_l$	$1.30(\xi_l + \xi_r)/2$	no
	0	$0.1667\xi_l$	—	yes
	$5 \cdot 10^{-6}$	$\xi_l$	$1.27\xi$	no
	$1.5 \cdot 10^{-3}$	$\xi_l$	$1.41\xi$	no
	$6.0 \cdot 10^{-3}$	$\xi_l$	—	yes
YO/GSA	0	$0.6\xi_l$	$1.19(\xi_l + \xi_r)/2$	no
	0	$0.1667\xi_l$	—	yes
	$5 \cdot 10^{-6}$	$\xi_l$	$1.14\xi$	no
	$1.5 \cdot 10^{-3}$	$\xi_l$	$1.17\xi$	no
	$6.0 \cdot 10^{-3}$	$\xi_l$	—	yes

Table 2: Summary of results for CR, AS, and YO. †: The difference of the two prominent peaks has been taken.

Although we still have concerns about the accuracy of WMPT we believe we have demonstrated that it is a method which deserves further consideration.

The motion of the beam centroids under the collective force shows two dominant modes if the separation of the unperturbed tunes  $\Delta Q$  is much smaller than the beam–beam tune shift parameter  $\xi$ . The modes are damped when  $\Delta Q$  is significantly larger than  $\xi$ . The relative separation  $(Q_\sigma - Q_\pi)/\xi$  depends not only on the model for the collective force but also on the separation of the unperturbed tunes  $\Delta Q$ . In the intermediate regime the results depend on the type of the limit under consideration. Moreover, our simulations suggest that the modes are damped when the ratio  $\xi/\xi^*$  differs strongly from 1. An onset of damping for  $\xi/\xi^* \approx 0.6$  could not be observed. The main results of sections 5.1 and 5.2 are summarized in Tab. 2

Only some aspects of the analysis have been presented. The way `BBDemo1D` keeps track of and stores different intermediate physical quantities (e.g. the macro–particle trajectories) allows a variety of post–simulation data analysis. Various post–processing facilities, e.g. for the Fourier analysis of the trajectories and for frequency maps for the moments as well as the trajectories have already been written and tested.

As a next step in the development phase of the code will be extended to 2–D motion. The basic structure of the code allows this to be done in a straightforward manner. Nevertheless, with a 4–D phase space computational speed is even more of an issue. Even an  $O(N)$  algorithm for the computation of the beam–beam kick is then already  $O(n^4)$  for a square mesh of  $N = n^4$  particles. Naive treatment of the collective force in the WMPT approach would, without GSA, lead to an  $O(N^2) = O(n^8)$  algorithm. Fortunately there exist 2–D Poisson solvers with an asymptotic order count of  $O(N)$  [GE88].

The results obtained with `BDeMo1D` will be cross checked with the PF operator method[WE00].

Finally we plan to implement long-range (parasitic) interactions, more IPs and complex filling schemes.

## 7 Acknowledgments

We gratefully acknowledge fruitful discussions with Bob Warnock.

One of the authors (M.V.) wishes to thank the members of the FNAL BD/BP group for the warm hospitality and the fruitful cooperation during his stay at FNAL.

The work of J.A.E. and M.V. was supported by US D.O.E. grant DE-FG03-99ER41104.

The work of T.S. was supported by US D.O.E. grant to Fermilab DE-AC02-76HO300.

## A Numerical Representation of the Yokoya–Koiso–Zenkevich Force

We start with the beam–beam kick assuming we know  $\psi_{\theta_c}^*$ .

$$\begin{aligned}
K_{\text{yo}}[\rho_{\theta_c}^*](q) &= \lim_{\epsilon \searrow 0} \left( \int_{q+\epsilon}^{+\infty} \frac{\rho_{\theta_c}^*(q')}{q-q'} dq' + \int_{-\infty}^{q-\epsilon} \frac{\rho_{\theta_c}^*(q')}{q-q'} dq' \right) \\
&= \lim_{\epsilon \searrow 0} \int_{\mathbb{R}^2 - \mathcal{A}_q(\epsilon)} \frac{\psi_{\theta_c}^*(\vec{z}')}{q-q'} d^2 z' \\
=: I_{\eta}^+(q) + I_{\eta}^-(q) &= \int_{\mathbb{R}^2 - \mathcal{A}_q(\eta)} \frac{\psi_{\theta_c}^*(\vec{z}')}{q-q'} d^2 z' + \lim_{\epsilon \searrow 0} \int_{\mathcal{A}_q(\eta) - \mathcal{A}_q(\epsilon)} \frac{\psi_{\theta_c}^*(\vec{z}')}{q-q'} d^2 z' \quad (\text{A.1})
\end{aligned}$$

where  $\mathcal{A}_q(x) = \mathbb{R} \times (q-x, q+x)$  is the (open) ribbon of width  $2x$  around  $q$ . In the last step we have split the domain of integration into two parts, In the first one ( $\mathbb{R}^2 - \mathcal{A}_q(\eta) \rightarrow I_{\eta}^+$ ) we can perform an ordinary numeric quadrature and in the second one ( $\mathcal{A}_q(\eta) - \mathcal{A}_q(\epsilon) \rightarrow I_{\eta}^-$ ) with  $\eta$  chosen suitably small, we can expand  $\psi_{\theta_c}^*$  around  $q$  w.r.t.  $q'$

$$\psi_{\theta_c}^*(q', p') = \sum_{l=0}^L \frac{\psi^{(l)}(q, p')}{l!} (q' - q)^l + O((q' - q)^{L+1}) \quad , \quad |q' - q| < \eta \quad . \quad (\text{A.2})$$

Since  $\mathcal{A}_q(\eta) - \mathcal{A}_q(\epsilon)$  is symmetric around  $q$  only the terms of  $\psi_{\theta_c}^*(q')/(q-q')$  which are even in  $q-q'$  contribute to the integral and we finally find

$$K_{\text{yo}}[\rho_{\theta_c}^*](q) = \int_{\mathbb{R}^2 - \mathcal{A}_q(\eta)} \frac{\psi_{\theta_c}^*(\vec{z}')}{q-q'} d^2 z' - 2 \int_{\mathbb{R}} \sum_{l=0}^{(L-1)\text{div}2} \frac{\psi^{(2l+1)}(q, p')}{(2l+1)!(2l+1)} \eta^{(2l+1)} dp' + O(\eta^L) \quad (\text{A.3})$$

where  $L' = L + 2$  if  $L$  is odd and  $L' = L + 1$  if  $L$  is even. Thus once  $\psi_{\theta_c^-}^*$  is known and its derivatives w.r.t.  $q'$  can be computed, e.g. by divided differences, up to the presumably *odd* order  $L$  then, the Cauchy principal value in  $K_{y_0}$  only adds to the overall numerical error of the integral to order  $O(\eta^{L+2})$ , where  $\eta$  is of the order of the (initial) mesh size. We note that in the case of known  $\psi_{\theta_c^-}^*$  and correspondingly known  $\rho_{\theta_c^-}^*$  we can *formally* simplify (A.3)

$$K_{y_0}[\rho_{\theta_c^-}^*](q) = \left( \int_{q+\eta}^{+\infty} + \int_{-\infty}^{q-\eta} \right) \frac{\rho_{\theta_c^-}^*(q')}{q - q'} dq' - 2 \sum_{l=0}^{(L-1)\text{div}2} \frac{\rho^{(2l+1)}(q)}{(2l+1)!(2l+1)} \eta^{(2l+1)} + O(\eta^{L'}) \quad . \quad (\text{A.4})$$

But we definitely need  $\psi^*$  for WMPT. There we have

$$\begin{aligned} K_{y_0}[\rho_{\theta_c^-}^*](q) &= \lim_{\epsilon \searrow 0} \int_{\mathbb{R}^2 - \mathcal{A}_q(\epsilon)} \frac{\psi_0^*(\vec{M}_{\theta_c^-}^{-1}(\vec{z}'))}{q - q'} d^2 z' \\ &= \lim_{\epsilon \searrow 0} \int_{\mathbb{R}^2 - \mathcal{B}_q(\epsilon)} \frac{\psi_0^*(\vec{z}')}{q - \vec{M}_{\theta_c^-}(\vec{z}')} d^2 z' \\ =: \tilde{I}_\eta^+(q) + \tilde{I}_\eta^-(q) &= \int_{\mathbb{R}^2 - \mathcal{B}_q(\eta)} \frac{\psi_0^*(\vec{z}')}{q - \vec{Q} \cdot \vec{M}_{\theta_c^-}(\vec{z}')} d^2 z' + \lim_{\epsilon \searrow 0} \int_{\mathcal{B}_q(\eta) - \mathcal{B}_q(\epsilon)} \frac{\psi_0^*(\vec{z}')}{q - \vec{Q} \cdot \vec{M}_{\theta_c^-}(\vec{z}')} d^2 z' \end{aligned} \quad (\text{A.5})$$

where  $\mathcal{B}_q(x) := \vec{M}_{\theta_c^-}^{-1}(\mathcal{A}_q(x))$  is the subset of  $\mathbb{R}^2$  so that for all  $\vec{z} \in \mathcal{B}_q(x)$ :  $\vec{M}_{\theta_c^-}(\vec{z}) \in \mathcal{A}_q(x)$  and  $\vec{Q} \cdot \vec{z}$  is the projection of  $\vec{z}$  onto configuration space. The integral  $\tilde{I}_\eta^+(q) = I_\eta^+(q)$  does not produce any algorithmic complication. It is given as sum over all the weighted macro-particles that at  $\theta_c^-$  fall *outside* of  $\mathcal{A}_q\eta$ . But  $\tilde{I}_\eta^-(q)$  is an integral that not only can have a fairly complicated domain due to the nonlinearity of  $\vec{M}_\theta$ , but the projection  $\tilde{\eta}$  of the set  $\mathcal{B}_q(\eta)$  on the  $q$ -axis even for arbitrarily small  $\eta$  *cannot* be guaranteed to be small. Therefore the truncated Taylor expansion (A.2) that lead to a good approximation of  $I_\eta^-(q)$  for small  $\eta$  cannot be applied to  $\tilde{I}_\eta^-(q)$ . As an example suppose  $\vec{M}_\theta$  to be linear and a simple rotation in phase space with angle  $Q\theta$  and basically irrational  $Q$ . Then already after the first turn ribbon  $\mathcal{B}_q(\eta)$  that is mapped to  $\mathcal{A}_q(\eta)$  has a finite tilt w.r.t. the  $q$ -axis and therefore in principle an infinite projection  $\tilde{\eta}$ . Of course in a simulation the integrals have a finite outer cut-off  $\pm p_{\max}$  and  $\pm q_{\max}$  those are naturally set to *large* values, say a couple of beam- $\sigma$ s and therefore do *not* guarantee small  $\tilde{\eta}$ .

Going back one step and using the first line of (A.5) does not help since there not  $\psi_{\theta_c^-}^*$  but  $\psi_0^* \circ \vec{M}_{\theta_c^-}^{-1}$  has to be expanded, leading to the same problem of the unbounded error.

Note that *mathematically* (A.5) is still well defined since, because of the volume preservation of  $\vec{M}_\theta$ , in the limit  $\epsilon \rightarrow 0$  with the measure of  $\mathcal{A}_q(\epsilon)$  also the measure of  $\mathcal{B}_q(\epsilon)$  goes to zero. Just its numerical representation has an error which cannot so easily be bounded.

Therefore in WMPT, the integral  $\tilde{I}_\eta^-(q)$  is not well represented. In the current version of BBDemo1D it is just approximated by  $\tilde{I}_\eta^-(q) = 0$  with a reasonably small  $\eta$ . The reason why  $\eta$  cannot be chosen arbitrarily small is that in order to get a good approximation of the Cauchy principle value one needs sufficiently large and basically equal relative densities of many macro-particles on both sides but close to the boundary of  $\mathcal{A}_q(\eta)$ . Otherwise single particles

being close to the boundary and not balanced by a particle “on the other side” will produce a strong and basically stochastic kick. It turned out during the simulation that the approximation  $K_{\text{yo}}[\rho_{\theta_c}^*](q) \approx \tilde{I}_\eta^+(q)$  destabilizes the beam in the used parameter range (see section 4). It has to be noted that the PF method, since it *does* have knowledge of a numerical approximation of  $\psi_{\theta_c}^*$  should in principle be more suitable to handle the Yokoya–Koiso–Zenkevich force.

## B The GSA for the Yokoya–Koiso–Zenkevich Force

The GSA for the Yokoya–Koiso–Zenkevich force leads to

$$K_{\text{yo}}[\rho](x) = \frac{\zeta}{\sqrt{2\pi}\sigma} \int \frac{e^{-\frac{(x'-\mu)^2}{2\sigma^2}}}{x-x'} dx' \quad . \quad (\text{B.1})$$

We now compute the Cauchy principle value using methods from complex variables.

We want to compute

$$f(x) := \frac{1}{\sqrt{\pi}} \int \frac{e^{-s^2}}{x-s} ds \quad . \quad (\text{B.2})$$

We consider the function

$$G(z) := \frac{1}{2\pi i} \int_{\mathbb{R}} \frac{e^{-s^2}}{s-z} ds \quad . \quad (\text{B.3})$$

Clearly  $G$  is holomorphic for  $\Im z \neq 0$ . Now let  $z =: x + iy$ . Then using Plemelj’s formula [AF97] we find

$$G(x + i0^\pm) = \pm \frac{1}{2} e^{-x^2} + \frac{1}{2\pi i} \int \frac{e^{-s^2}}{s-z} ds \quad . \quad (\text{B.4})$$

We now define

$$F(z) := G(z) \quad , \quad \Im z < 0 \quad (\text{B.5a})$$

$$:= -\frac{1}{2} e^{-x^2} - \frac{1}{2\sqrt{\pi}i} f(x) \quad , \quad \Im z = 0 \quad (\text{B.5b})$$

$$:= -e^{-z^2} + G(z) \quad , \quad \Im z > 0 \quad (\text{B.5c})$$

Note that  $F$  is holomorphic for  $\Im z \neq 0$  and continuous for  $\Im z = 0$ . It follows (see, e.g. theorem 3.2.7 of [AF97]) that  $F$  is entire. Moreover note that

$$F(z) = \frac{1}{2\pi i} \int_{\mathcal{C}} \frac{e^{-s^2}}{s-z} ds \quad (\text{B.6})$$

where  $\mathcal{C}$  is a Landau contour described in Fig. 9.

Differentiating  $G$  for  $\Im z < 0$ , integrating by parts and using  $s/(s-z) = z/(s-z) + 1$  we find

$$G'(z) = \frac{1}{2\pi i} \int_{\mathbb{R}} \frac{e^{-s^2}}{(s-z)^2} ds$$

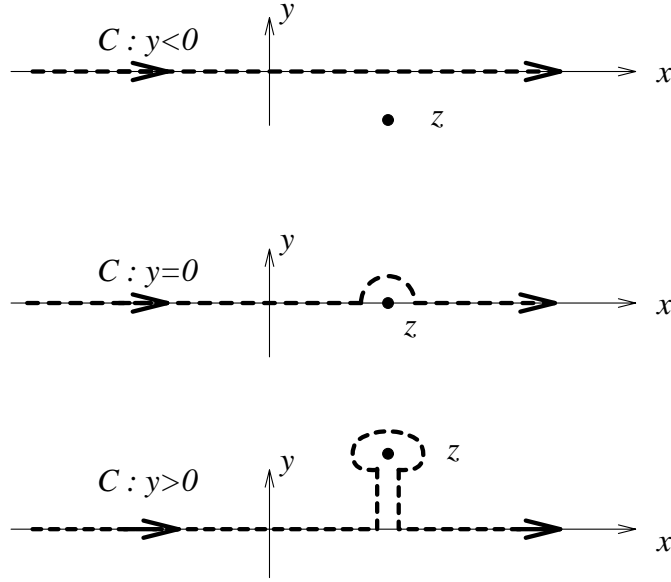


Figure 9: The Landau contour.

$$\begin{aligned}
&= \frac{1}{2\pi i} \left( \frac{-e^{-s^2}}{s-z} \Big|_{-\infty}^{+\infty} - \int_{\mathbb{R}} \frac{2s e^{-s^2}}{s-z} ds \right) \\
&= \frac{-1}{\pi i} \int_{\mathbb{R}} \left( \frac{e^{-s^2}}{s-z} + e^{-s^2} \right) ds = -2z G(z) - \frac{1}{\sqrt{\pi} i}
\end{aligned} \tag{B.7}$$

It follows that

$$F' + 2z F = \frac{i}{\sqrt{\pi}} \tag{B.8}$$

for all  $z \in \mathbb{C}$  since if 2 entire functions are equal on an open subset of  $\mathbb{C}$ , they are equal on  $\mathbb{C}$ . Now because of (B.5b) and (B.2), and since  $e^{-s^2}$  is even whereas  $1/s$  is odd we find that  $f$  is a solution of the initial value problem

$$f' + 2x f = 2 \quad , \quad f(0) = 0 \quad . \tag{B.9}$$

Note that if one differentiates  $f$  defined by (B.2) and then “bravely” interchanges the differentiation with the limit of the Cauchy principle value, then one obtains (B.9) following the procedure in (B.7).

One easily verifies that

$$f(x) = 2 e^{-x^2} \int_0^x e^{t^2} dt = \sqrt{\pi} \mathfrak{S} W(x) \quad , \tag{B.10}$$

where  $W$  is the complex “error” function [GR81, CL01], solves (B.9).

Finally replacing  $x$  by  $(x - \mu^*)/(\sigma^* \sqrt{2})$  yields the expression in (3.37).

## C Conventions and Used Symbols

Let  $X$  be a quantity of one beam, then  $X^*$  is the same quantity for the other beam. A more old-fashioned notation would be using  $X^{(1)}$  and  $X^{(2)}$ . We want to stress the point that the beam–beam interaction is *formally* symmetric and thus from any equation including lattice- and beam–beam effects for *one* beam we immediately obtain the corresponding equation for the *other* beam by toggling the asterisk on all relevant parameters and dynamical variables.

Symbol	Comment
$\theta$	generalized machine azimuth
$\theta_c$	azimuth of collision point
$f(\theta_c^-), f(\theta_c^+)$	$\lim_{\theta \nearrow \theta_c} f(\theta), \lim_{\theta \searrow \theta_c} f(\theta)$
$q, x, y, r$	spatial coordinate (in general, hor., vert., “radial”)
$p$	conjugate momentum ( $\vec{z} \equiv (q, p)$ )
$\sigma_0$	initial rms beam width
$\psi_\theta(q, p)$	phase space density (normalized to 1) at $\theta$
$\rho_\theta(q)$	spatial density (normalized to 1) at $\theta$
$\tilde{\rho}(q; \{\text{parameters}\})$	test density ( $\rightarrow$ GSA)
$\rho(q; \mu, \sigma)$	Gaussian with $\mu := \langle q \rangle, \sigma^2 := \langle (q - \mu)^2 \rangle$
$\vec{R}$	linear lattice map
$\underline{R}$	Jacobian of linear lattice map
$Q_0, \beta_0, \alpha_0, \gamma_0$	tune & Courant–Snyder fcts. due to linear lattice
$\vec{K}$	beam–beam kick map
$K[\rho](q)$	kick function (i.e. $p \rightarrow p + K[\rho](q)$ )
$\tilde{G}(q, q')$	Green’s function of Poisson eq.
$G(q, q')$	(CR/YO: $\equiv \partial_q \tilde{G}(q, q')$ ) beam–beam kernel
$\tilde{K}(q; \{\text{parameters}\})$	kick function using test density ( $\rightarrow$ GSA)
$\underline{K}$	Jacobian of beam–beam kick map
$\kappa[\rho](q)$	( $\equiv (\underline{K})_{21}$ ) linearized kick function (i.e. $K[\rho](q) = \kappa[\rho]q + O(q^2)$ )
$\xi$	linear beam–beam tune shift parameter
$\zeta$	( $\equiv \zeta(\xi)$ ) proportionality factor in beam–beam kick
$\vec{T}$	one turn map
$\underline{T}$	Jacobian of OTM
$\vec{M}_\theta$	map from 0 to $\theta$
$\mathfrak{T}$	Perron–Frobenius operator
$\mathfrak{X}$	projector on spatial coordinate(s)
$\vec{z}_{ij}$	( $\equiv (q_i, p_j)$ ) mesh point
$\vec{\eta}_{ij}(\theta)$	( $\equiv \vec{M}_\theta(\vec{z}_{ij})$ ) trajectory starting at mesh point
$\mathfrak{W}_{ij}$	total weight of a trajectory
$\chi(\mu, q, q')$	indicator function of $[\mu - q, \mu + q]$
$\chi_{\mu, \nu}(\vec{z})$	indicator function of bin $(\mu, \nu)$
$n$	number of particles per phase space dimension
$N$	number of particles in initial mesh ( $\equiv n^2$ for 1 d.o.f.)
$\mathbb{R}, \mathbb{R}^2$	configuration space, phase space
$\mathcal{A}$	(mathcal font!) some set (e.g. $\mathcal{A} \subset \mathbb{R}^2$ , etc.)
$f$	Cauchy principal value
$a := b, a =: b, a \equiv b$	$a$ defined by $b, b$ defined by $a, a$ and $b$ identical by def.

## References

- [AF97] M. J. Ablowitz and A. S. Fokas, *Complex Variables*, Cambridge University Press (1997)
- [AL99] Y. Alexahin, *Proc.: LHC99 Beam-Beam WS., CERN*, pp. 41-44, (1999)
- [AN98] E. B. Anderson, Dissertation, Cornell University (1998)
- [CL01] CERNLIB, short writeups,  
<http://wwwinfo.cern.ch/asdoc/cernlib.html>
- [CR85] A. W. Chao and R. D. Ruth, *Part.Acc.* **16**, pp. 201-216 (1985)
- [EW01] J. A. Ellison and R. L. Warnock, *Proc.: 2-nd ICFA Workshop on Auantum Aspects of Beam Phsyics*, Capri, Oct. 2000, to be published by World Scientific; also available as: SLAC-PUB-8778
- [FU98] M. A. Furman, *Proc.: International Computational Accelerator Physics Conference*, Monterey, (1998)
- [GE88] L. Greengard, *Thesis*, The MIT PRes Cambridge MA London England (1988)
- [GR81] I. Gradstein and I. Ryshik, *Tables of Series, Products and Integrals*, Verlag Harri Deutsch, Thun, Frankfurt am Main (1981)
- [HO99] A. Hoffman, *Proc.: LHC99 Beam-Beam WS., CERN*, pp. 56-58, (1999)
- [HO00] G. H. Hoffstaetter, in proceedings of EPAC 2000 Vienna, (2000)
- [KA92] S. K. Kauffmann et al., *Proc.: Advanced Beam Dynamics Workshop on Effects of Errors in Accelerators*, Ed.: A. Chao, AIP Conf. Proc. 255, (1992)
- [KR00] S. Krishnagopal, *Phys.Rev.S.T.-AB* **3** 024401 (2000)
- [LH00] LHC Conceptual Design, CERN/AC/95-05, (1995)
- [NR92] W. H. Press, S. A. Teukolsky, W. T. Vetterling and B. P. Flannery, *Numerical Recipes in FORTRAN, 2-nd Ed.*, Cambridge University Press (1992)
- [TE00] Tevatron Run-II Handbook, FNAL, unpublished.
- [WE00] R. L. Warnock and J. A. Ellison, *Proc.: 2-nd ICFA WS. on High Brightness Beams, UCLA*, Ed.: J. Rosenzweig and L. Serafini, World Scientific, (2000); also available as preprint SLAC-PUB-8404
- [VL01] VLHC Design Study, <http://www.vlhc.org>, (2001)
- [WO96] S. Wollman and E. Ozizmir, *SIAM J.Numer.Anal.* **33** #4, pp. 1377-1409 (1996)
- [WO99] S. Wollman, *J.Comp.Appl.Math.* **115**, pp. 593-600 (1999)

- [WO00] S. Wollman, *SIAM J.Numer.Anal.* **37** #4, pp. 1369–1398 (2000)
- [YK90] K. Yokoya and H. Koiso, *Part.Acc.* **27**, pp. 181–186 (1990)
- [YZ93] K. Yokoya and P. Zenkevich, *Part.Acc.* **40**, pp. 229–241 (1993)
- [ZZ99] M.–P. Zorzano and F. Zimmermann, *LHC Project Report* **314**, CERN/SL (1999)